193 (2024) 206972

Contents lists available at ScienceDirect

Applied Catalysis O: Open

journal homepage: www.elsevier.com/locate/apcato

Influence of Cu:Fe ratio in synthesis of higher alcohols from syngas over CuFeCoK/attapulgite catalysts

Atte Aho [a], Noora Lind [a], Pasi Virtanen [a], Päivi Mäki-Arvela [a], Kari Eränen [a], Sari Granroth [b], Ville Korpelin [c], Karoliina Honkala [c], Vincenzo Russo [d], Irina Simakova [a], Dmitry Yu. Murzin [a,*]

[a] Laboratory of Industrial Chemistry and Reaction Engineering, Johan Gadolin Process Chemistry Centre, Åbo Akademi University, Åbo, Finland
[b] Department of Physics and Astronomy, University of Turku, Turku, Finland
[c] Department of Chemistry, University of Jyväskylä, Jyväskylä, Finland
[d] Università di Napoli Federico II, Napoli, Italy

ARTICLE INFO

Keywords:
Syngas
Higher alcohols
Copper
Iron
Attapulgite

ABSTRACT

Synthesis of higher alcohols from syngas (H_2:CO ratio 2 and 1) was performed at 225–300 °C and 30 bar over copper, iron and cobalt containing catalysts supported on attapulgite and promoted with potassium. The Cu:Fe ratio was varied to study its influence on the syngas conversion and product distribution. It was found that while the copper rich catalyst 17Cu3FeCoK/attapulgite resulted in higher selectivity to the undesired alkanes with methane as the major one, the iron rich 3Cu17FeCoK/attapulgite was more selective towards alkenes. Selectivity to CO_2 was independent on the Cu:Fe ratio tested in this work. With the higher H_2:CO ratio (i.e. 2) selectivity to the liquid products increased with the increasing iron content. Moreover, a higher iron content in the catalyst improved formation of higher alcohols while the α-value reflecting the chain growth probability was more or less independent on the catalyst type.

1. Introduction

Higher alcohols, i.e. ethanol and longer carbon chain alcohols [1–3], are utilized in various chemical applications such as intermediates in pharmaceuticals and other fine chemicals as well as in the energy sector. The higher alcohols can be produced in various ways, with the most common way being fermentation of sugars to ethanol, other ways include hydration of alkenes and catalytic conversion of syngas [2,4]. Syngas or synthesis gas, is a mixture of hydrogen and carbon monoxide, generally produced through steam reforming, partial oxidation or gasification of various feedstock.

The catalysts used for syngas conversion to higher alcohol synthesis (HAS) can be divided into four groups namely Rh-based, Mo-based, modified methanol synthesis catalysts, and modified Fischer-Tropsch iron and cobalt catalysts [2,4–6]. During HAS from syngas other reactions can also occur, namely, formation of alkanes and alkenes as well as the water gas shift reaction (WGSR) according to the equations below.

$$n{\cdot}CO + 2n{\cdot}H_2 \rightarrow C_nH_{2n+1}OH + (n-1){\cdot}H_2O \quad \text{alcohols}$$

$$n{\cdot}CO + (2n+1){\cdot}H_2 \rightarrow C_nH_{2n+2} + n{\cdot}H_2O \quad \text{alkanes}$$

$$n{\cdot}CO + 2n{\cdot}H_2 \rightarrow C_nH_{2n} + n{\cdot}H_2O \quad \text{alkenes}$$

$$CO + H_2O \leftrightarrow CO_2 + H_2 \quad \text{water gas shift reaction}$$

The Rh-based catalysts are often promoted with alkali or other transition metals, with manganese being a typical promoter, to improve the selectivity to higher alcohols [6,7]. Mao et al. [8] studied the influence of Mn on Rh/SiO_2 catalyst in the synthesis of C_{2+} oxygenates from syngas. A clear promotional effect of Mn was reported, as the conversion of CO increased from 5% to 17% with a 1.5Rh-0.4Mn (wt-%) catalyst compared to the monometallic Rh/SiO_2 counterpart. Furthermore, selectivity to the undesired CH_4 decreased from over 70% to <40% and selectivity to the desired oxygenates increased from 17% to 47%, with the main oxygenates being ethanol and acetic acid. Yu et al. [9] studied the effect of iron addition to a multimetallic Rh-Mn-Li/SiO_2 catalyst. The authors [9] reported that small concentrations (<0.1%) of iron had a beneficial effect on the CO conversion and selectivity to oxygenates (with ethanol and acetic acid as the main oxygenates), while a higher iron loading had an opposite effect. Supports other than SiO_2

* Corresponding author.
E-mail address: dmitry.murzin@abo.fi (D.Yu. Murzin).

https://doi.org/10.1016/j.apcato.2024.206972
Received 14 May 2024; Received in revised form 26 June 2024; Accepted 28 June 2024
Available online 2 July 2024

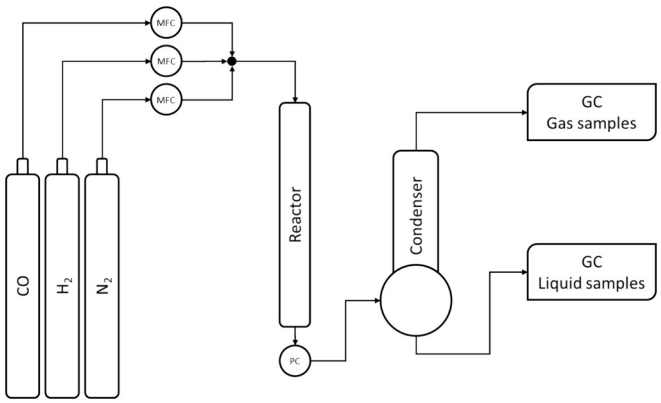

Fig. 1. Reactor set-up scheme.

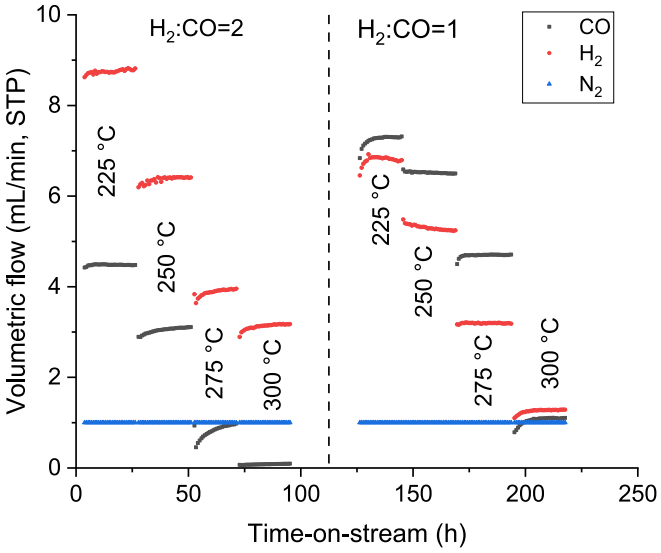

Fig. 2. Time-on-stream plot for the reacting gases and the internal standard, nitrogen with the use of 12Cu8FeCoK/attapulgite as a catalyst.

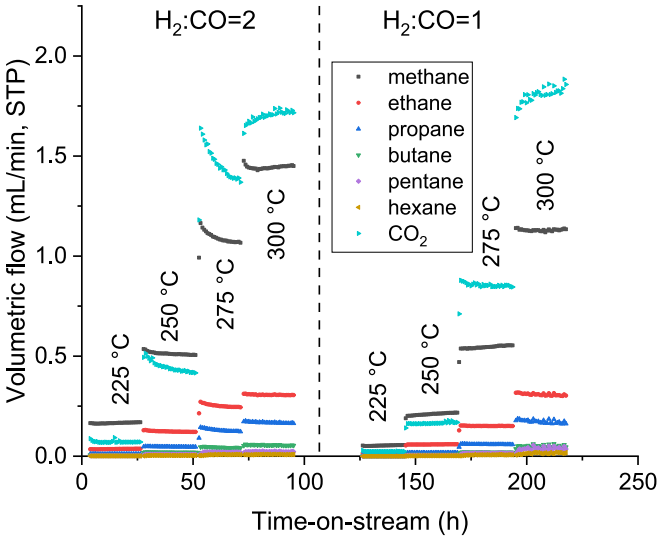

Fig. 3. Time-on-stream plot for the volumetric flow of the formed alkanes and CO_2 with the use of 12Cu8FeCoK/attapulgite as a catalyst.

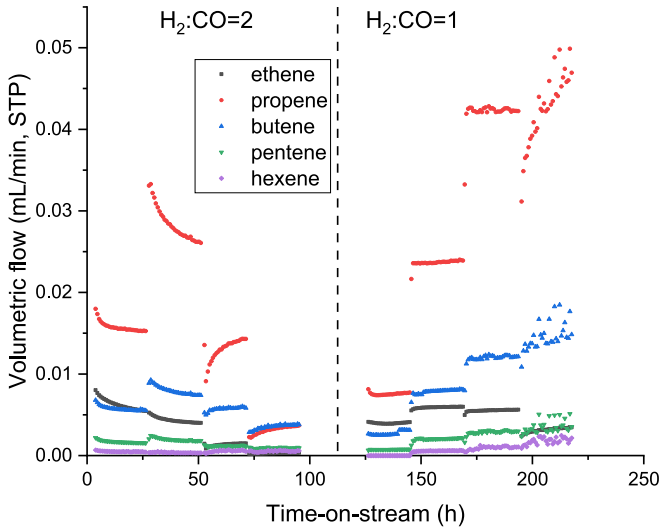

Fig. 4. Time-on-stream plot for the volumetric flow of the formed alkenes with 12Cu8FeCoK/attapulgite as a catalyst.

have also been used for the Rh-based catalysts, namely ZrO_2, CeO_2 and MgO [10], synthetized through co-precipitation of metal nitrates with $NH_3{\cdot}H_2O$ as the precipitating agent. Liu et al. [10] reported that over $Rh/Ce_{0.8}Zr_{0.2}O_2$ ethanol was formed with selectivity exceeding 35%. It can be concluded, based on the literature [8–10] that, typical for the Rh-based catalysts is the formation of ethanol and acetic acid as well as low selectivity to CO_2 which can be as low as 1–2%.

The Mo-based catalysts can be divided into MoS_2, Mo_2C, MoO_x and MoP [4,11]. A clear difference between the Mo-based and Rh-based catalysts is that the former one generate significantly more methanol [4]. Boahene et al. [12] used a K-doped $CoRhMo_2S$/MWCNT catalyst and reported very high 85.7% selectivity to alcohols with selectivity to methanol of 22.1%, low selectivity to hydrocarbons of ca. 6% and fairly low to CO_2 of 8.4%.

Modified methanol synthesis catalysts can be divided into low temperature catalysts with copper as the active metal and high temperature catalysts with chromium as the active metal [4]. Typically, these catalysts are promoted with iron, nickel, molybdenum, cobalt, lanthanum and manganese as well as various alkali metals. The modified methanol synthesis catalysts are usually selective for alcohol formation with low selectivity to hydrocarbons and CO_2. However, the selectivity to higher alcohols is rather low in most cases [13–15].

Modified Fischer-Tropsch (FT) catalysts for HAS contain either cobalt or iron as the active metals along with alkali and/or transition metals as promotors [4,16,17]. Compared to the other catalyst types mentioned above, the modified FT catalysts have some advantages, such as lower costs of the active metals, higher activity and selectivity to higher alcohols [18]. Copper modified FT catalysts have been used in the research on mixed (higher) alcohol synthesis, namely CuFeCo supported on attapulgite and promoted with potassium [19]. Attapulgite, a crystalline hydrated magnesium silicate material, is a naturally occurring clay with a fibrous or in some cases flake like morphology, characterized by a porous crystalline structure comprising tetrahedral layers alloyed together along longitudinal sideline chains subsequently making it an interesting option as a catalyst support material [20–22]. The catalysts applied by Guo et al. [19] resemble the ones that were tested in this work, being prepared through incipient wetness impregnation of metal nitrates on H_2SO_4 activated attapulgite and calcined at 400 °C in air. Guo et al. [19] synthesized catalysts with different metal loadings 20–70 wt% and five different Cu:Fe molar ratios ranging from 9.4/0.6 to 0.5/9.5 with 60% total metal loading and tested them at 350 °C, 55 bar, H_2:CO = 2 and GHSV of 6000 h^{-1}. The authors reported that a total metal loading of 60% was optimal for generating a high space time yield

Table 1
Conversion of CO and H_2 as well as selectivity to individual gas phase products including alkanes, alkenes and CO_2 for tested catalysts at different reaction temperatures and H_2:CO ratios. Selectivity to liquid products is calculated by the difference*.

Catalyst	Temperature (°C)	H_2:CO	CO	H_2	methane	ethane	propane	butane	pentane	hexane	ethene	propene	butene	pentene	hexene	CO_2	liquid
12Cu8FeCoK	225	2	14.3	16.9	22.4	9.8	4.6	3.0	1.8	1.0	1.6	6.2	3.0	1.1	0.4	9.6	35.5
	250	2	41.2	42.9	23.7	11.4	6.6	3.7	2.3	1.1	0.4	3.8	1.4	0.4	0.1	20.0	25.1
	275	2	83.4	76.4	24.8	11.5	8.8	4.1	2.4	1.1	0.1	0.9	0.5	0.1	0.1	33.0	12.6
	300	2	98.3	86.2	28.1	11.9	9.7	4.3	2.3	1.1	0.0	0.2	0.3	0.1	0.1	33.3	8.6
	225	1	7.2	13.3	9.7	5.1	2.1	1.5	1.0	0.6	1.4	4.0	2.0	0.7	0.0	4.3	67.5
	250	1	17.0	35.0	16.0	8.9	4.0	2.7	1.9	1.0	0.9	5.3	2.4	0.8	0.3	12.5	43.4
	275	1	40.1	70.1	17.5	9.6	5.7	2.6	2.6	1.4	0.4	4.0	1.5	0.5	0.2	27.1	27.1
	300	1	86.1	107.0	16.7	9.1	7.6	3.0	3.0	1.5	0.1	2.0	0.9	0.3	0.2	27.0	28.6
3Cu17FeCoK	225	2	31.3	32.7	16.2	9.2	5.0	3.5	2.3	1.4	1.3	6.8	3.5	1.7	0.7	14.4	34.2
	250	2	77.1	69.2	16.9	10.2	7.0	0.8	2.9	1.8	0.2	4.0	1.6	0.7	0.2	29.1	24.6
	275	2	98.4	82.9	20.0	10.7	10.2	4.2	3.6	2.0	0.0	1.0	0.7	0.2	0.1	33.2	14.1
	300	2	99.0	87.2	27.9	12.0	11.0	4.4	3.0	1.4	0.0	0.3	0.4	0.1	0.1	33.2	6.1
	225	1	10.0	16.0	10.1	6.4	3.2	2.4	2.0	2.0	2.1	6.2	3.4	1.6	0.8	6.4	53.7
	250	1	27.7	49.5	12.9	8.7	4.2	3.0	2.4	1.5	1.3	6.9	3.5	1.6	0.7	17.7	35.8
	275	1	66.7	97.8	11.9	8.2	4.8	2.3	2.8	1.7	0.4	5.2	2.3	1.0	0.5	34.1	24.6
	300	1	99.0	111.0	13.8	7.9	8.2	3.2	3.7	2.0	0.0	1.7	1.0	0.3	0.3	21.1	36.9
17Cu3FeCoK	225	2	4.2	5.6	27.6	7.5	3.4	2.4	0.2	0.0	2.8	5.8	3.3	0.8	0.0	6.9	39.2
	250	2	13.7	16.2	30.4	10.1	4.5	2.7	1.5	0.7	0.7	4.4	1.7	0.4	0.0	12.0	30.9
	275	2	36.7	40.4	33.4	10.8	6.5	2.9	1.5	0.6	0.2	1.8	0.6	0.1	0.0	20.2	21.3
	300	2	71.7	71.7	36.9	11.0	7.6	2.8	1.4	0.5	0.0	0.4	0.3	0.0	0.1	29.6	9.4
	225	1	3.8	4.4	7.2	2.1	0.9	0.6	0.0	0.0	1.0	1.7	1.3	0.0	0.0	2.8	82.4
	250	1	7.1	12.6	16.7	5.6	2.1	1.4	0.9	0.0	0.8	3.4	1.6	0.4	0.0	5.8	61.3
	275	1	17.1	33.6	25.2	8.8	4.3	2.4	1.5	0.6	0.4	3.6	1.3	0.2	0.0	14.1	37.6
	300	1	38.4	69.6	27.7	9.9	6.5	2.3	1.8	0.7	0.2	2.1	0.7	0.1	0.1	26.4	21.5

* Only n-alkanes and linear alpha-olefins were used in the calibration.

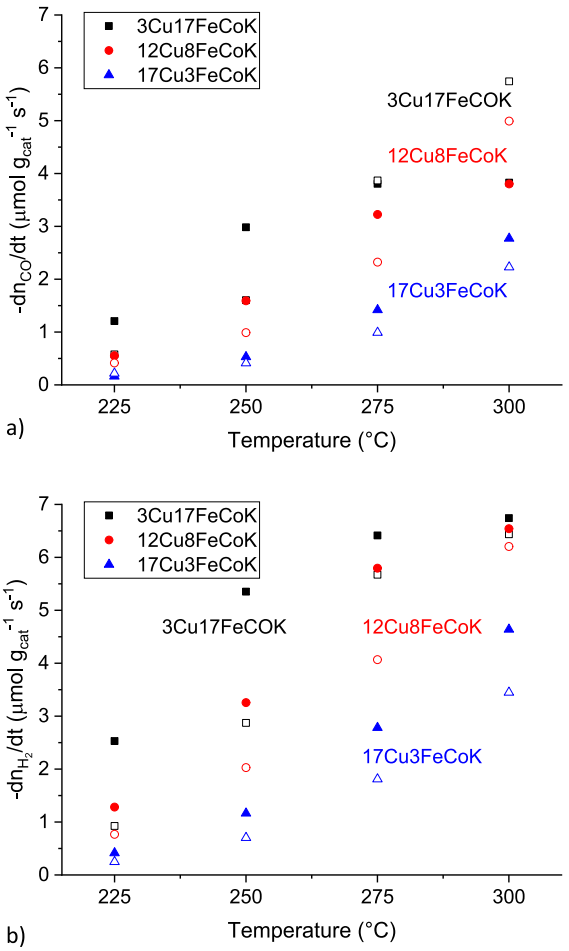

Fig. 5. Reaction rates (µmol g_{cat}^{-1} s^{-1}) of a) CO and b) hydrogen as a function of reaction temperature. H_2:CO = 2 is presented as closed symbols whereas open symbols reflect the lower ratio (1).

of the mixed alcohols, high CO conversion and high WGSR selectivity with a 5.2/4.8 Cu:Fe catalyst. The catalysts with various Cu:Fe ratios performed slightly differently, in a way that the high copper content catalyst ($Cu_{9.4}Fe_{0.6}$) produced alcohols with the lowest α-value (0.254) reflecting the chain growth probability, while the high iron content catalyst ($Cu_{0.5}Fe_{9.5}$) gave the highest α-value (0.375). Furthermore, the ratio of higher alcohols to methanol increased from 0.79 to 1.67 with increasing the iron content. CO conversion was found to increase with a higher iron content and reaching a plateau at $Cu_{5.2}Fe_{4.8}$, while a high copper content catalyst was more selective towards methane than the other catalysts.

The aim of this work is to prepare CuFeCoK/attapulgite catalysts and study the influence of the Cu:Fe ratio on the higher alcohol synthesis, in particular on the gas and liquid phase product distributions, under broad reaction condition ranges. The main aim was to study the influence of Cu to Fe ratio on catalytic performance, while cobalt was introduced in the catalyst composition as it is known to promote chain growth. Potassium is often added to the Fischer-Tropsch catalysts as a donor of electrons to iron promoting CO bond scission.

2. Experimental

2.1. CuFeCoK/attapulgite catalyst preparation

Attapulgite supported CuFeCoK catalysts were prepared by the wet impregnation. An aqueous solution (2–5 mL) containing appropriate amounts of $Cu(NO_3)_2{\cdot}3H_2O$ (Reachim, 98%), $Fe(NO_3)_3{\cdot}9H_2O$ (Sigma

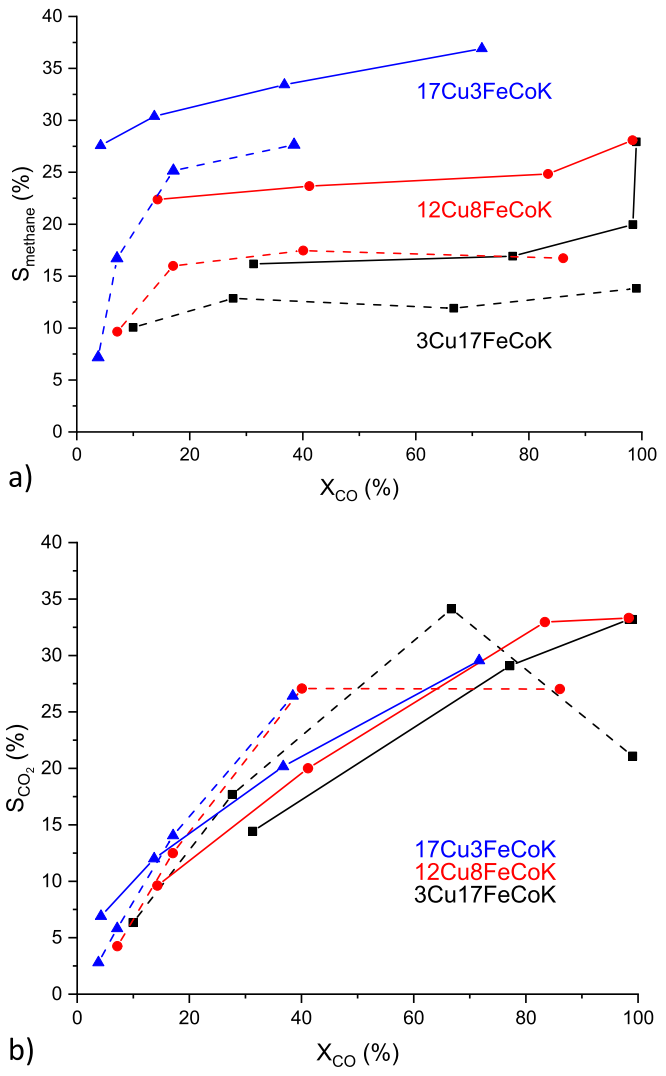

Fig. 6. Selectivity to a) methane and b) CO_2 as a function of CO conversion for different catalysts and different H_2:CO ratios, solid line ratio 2, dashed line ratio 1.

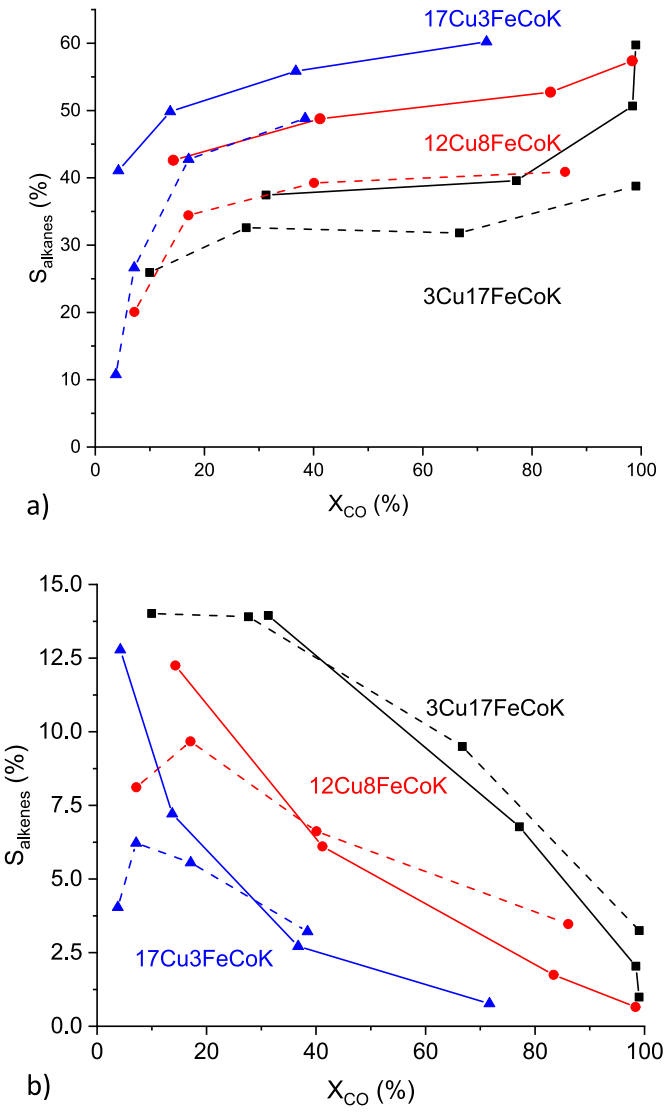

Fig. 7. Selectivity to alkanes (a) and alkenes (b) as a function of CO conversion for tested catalysts and different H_2:CO ratios, solid line ratio 2, dashed line ratio 1.

Aldrich, 99%), $Co(NO_3)_2{\cdot}6H_2O$ (Reachim, 98%) and KNO_3 (Reachim, 98%) was added dropwise to the attapulgite powder at room temperature by several portions followed by vacuum drying between additions. The resulting solid was dried in an oven at 100 °C for 17 h and thereafter calcined in static air at 450 °C (2 °C/min) for 6 h.

2.2. Catalyst characterization

2.2.1. XRD

Powder XRD patterns were obtained on a STOE STADI MP (STOE, Germany) diffractometer (Mo Kα radiation, λ = 0.7093 Å) equipped with a MYTHEN2 1 K sensitive detector. The data were collected in the 2θ range of 4°-30° with a step of 0.015° and a collection time of 3 s. The phase identification was performed using the ICDD PDF-2 database [Powder Diffraction File database PDF-2, International Centre for Diffraction Data, USA, 2009]. The dimensions of the coherently scattering domain (CSD - D_{XRD}) were determined as broadening of the diffraction peaks taking into account the instrumental broadening of diffraction lines estimated from diffraction picture of the international standard - LaB_6 (SRM 660c) at the same conditions. The average crystallite size of different phases was calculated by the line broadening analysis according to the Scherrer equation.

2.2.2. TEM-EDX

The structure and microstructure of the catalyst samples with different Cu/Fe ratio were studied by high-resolution transmission electron microscopy (HRTEM) using a ThemisZ electron microscope (Thermo Fisher Scientific, USA) with an accelerating voltage of 200 kV and a limiting resolution of 0.07 nm. Images were recorded using a Ceta 16 CCD matrix (Thermo Fisher Scientific, USA). The device is equipped with a SuperX (Thermo Fisher Scientific, USA) energy-dispersive characteristic X-ray spectrometer (EDX) with a semiconductor Si detector (an energy resolution 128 eV). For HRTEM analysis catalyst particles were uniformly deposited on perforated carbon support attached to copper grid using an ultrasonic disperser UZD-1UCH2.

2.2.3. N_2-physisorption

The specific surface area of the catalysts was measured through nitrogen physisorption using a Micrometrics MicroActive 3Flex 3500 instrument. Prior to the surface area measurements, the catalyst samples were outgassed at 250 °C for 4 h. The BET equation was used for calculating the specific surface area and NLDFT for the pore size distribution.

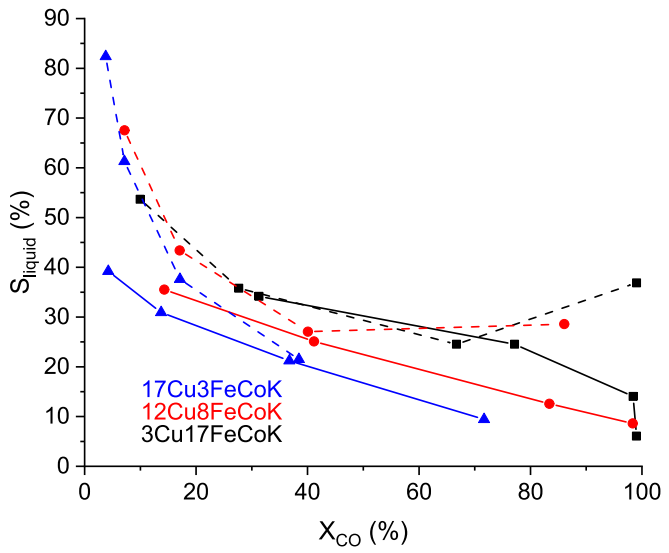

Fig. 8. Selectivity to the liquid products as a function of CO conversion for the different catalysts and H_2:CO ratios, solid line ratio 2, dashed line ratio 1.

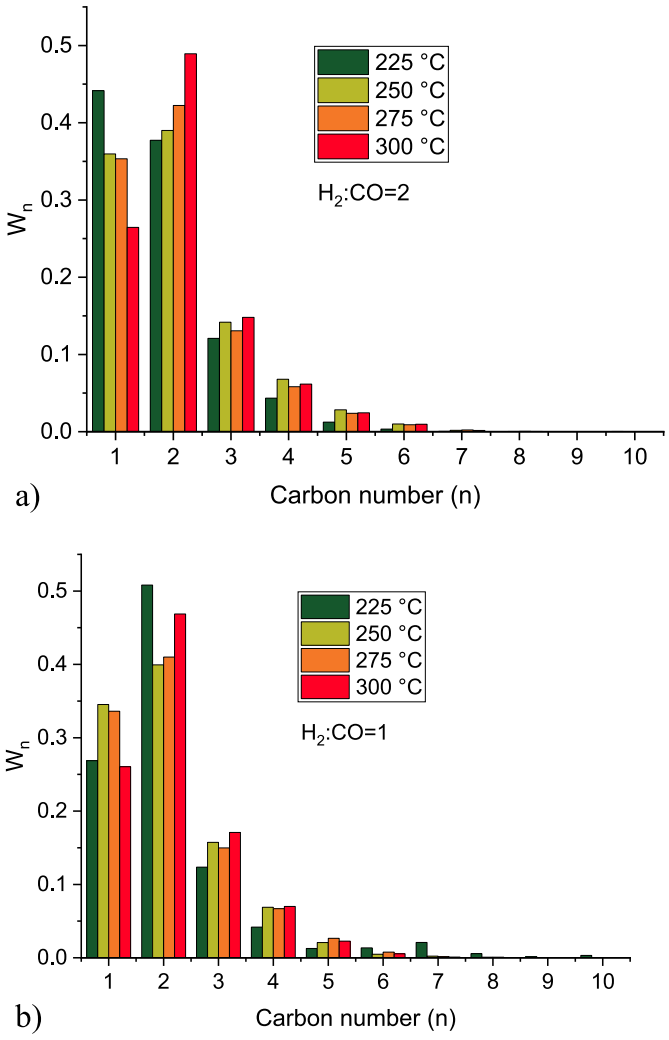

Fig. 9. The weight fraction of the alcohols formed during synthesis of higher alcohols over 12Cu8FeCoK/attapulgite catalyst at different temperatures and H_2:CO ratios of a) 2, b)1.

2.2.4. XPS

The oxidation states of copper and iron were determined by X-ray photoelectron spectroscopy using a NEXSA XPS (Thermo Fischer Scientific) for the fresh and spent catalysts. Al Kα radiation was used for the measurements with a spot size of 400 μm. Peak fitting was made with XPSPeak4.1 software, prior to peak fitting the Shirley background was subtracted from the data. Si2p peak of the support material was used as a reference peak to take possible sample charging into account.

2.2.5. TPR

Temperature programmed reduction (TPR) was studied with a Microtrac MRB, Belcat II device. The catalyst sample (50 mg) was dried in the sample holder tube at 200 °C in a 30 mL/min flow of argon. TPR was carried out from 35 °C to 700 °C with a heating rate of 10 °C/min in a 30 mL/min flow of 5% hydrogen in argon.

2.2.6. Reactor set-up and experimental procedure

The reactor set-up consisted of a stainless steel reactor tube with an inner diameter of 6 mm and a total length of 35 cm. The reactor tube was placed in an aluminum block inside the oven (Carbolite) to ensure better heat transfer. The temperature of the oven and the catalyst bed were monitored by K-type thermocouples. The gas flows of hydrogen (Woikoski N50), carbon monoxide (Air Liquide 3.7) and nitrogen (Woikoski N50) were controlled by the Brooks Instrument mass flow controllers (MFC). Nitrogen was used as an internal standard in the flow calculations, due to the non-equimolar reactions taking place. The pressure in the set-up was controlled with a backpressure regulator (Equilibar). Downstream the regulator, the formed alcohols were condensed at −15 °C and the gases eluting through the condenser were analyzed by an on-line GC (HP 6890 Series) equipped with both HP-PLOT-Q and HP-MOLSIV columns as well as TC and FI detectors for separation and analysis of CO, H_2, N_2, C1-C6 alkanes and C2-C6 alkenes along with CO_2. A scheme of the set-up is displayed in Fig. 1.

The reactor tube was filled by packing quartz wool in the bottom followed by glass beads (Sigma, 425–600 μm) to get the catalyst bed approximately to the middle height of the tube. The catalyst (0.5 g) was diluted with the equal amount of the glass beads and finally the remaining part of the tube was filled with glass beads. Quartz wool was packed between every beds to avoid mixing of the layers.

After filling the reactor tube and placing it in the aluminum block, the tube was attached to the set-up. Thereafter, the set-up was pressurized with nitrogen and carefully checked for possible leakages. When it was ensured that no leakage was present, the pressure was released to atmospheric pressure. Prior to starting the catalyst testing, the catalysts were reduced for 3 h in 10 mL/min (STP) hydrogen flow followed by carburization for 3 h with 10 mL/min (STP) CO flow at 300 °C. It has been reported [23] that carburization with CO increases the CO conversion in FT synthesis with a low alpha iron catalyst as the transformation of iron into χ-Fe_5C_2 is enhanced compared to other pretreatment methods. Iron carbides have been reported to act as the active sites for CO dissociation and chain propagation [3]. After carburization the gas was switched to nitrogen and the temperature was lowered to 225 °C. Testing of a catalyst was started at 225 °C by feeding a gas mixture containing 6% nitrogen and hydrogen and carbon monoxide with a ratio of 2 using the gas hourly space velocity (GHSV) of 2000 mL h^{-1} g_{cat}^{-1}. The pressure was increased to 30 bar after flushing the reactor with the reaction gas mixture for approximately 30 min. Different reaction temperatures were tested namely, 225, 250, 275 and 300 °C, each temperature was kept for 24 h with continuous on-line analysis of the gases and collecting one liquid sample at each temperature. Later during the run, the H_2/CO ratio was changed to 1 keeping the concentration of nitrogen and GHSV constant.

2.2.7. Product analysis

Online analysis of the eluting gas stream was done with the GC described above. The responses from TC and FI detectors were calibrated

Table 2
Comparison of the performance of different catalysts in syngas transformation to higher alcohols.

Entry	Catalyst	Reaction Conditions				CO conversion [%]	STY_{OH} [$g/g_{cat}.h$]	S_{CO2} [%]	S_{CH4} [%]	S_{ROH} [%]	S_{HC} [%]	Reference
		T [°C]	P [MPa]	H_2/CO	GHSV [$mL/g_{cat}.h$]							
1	Co_1Fe_4@ZrO_2–10	245	5.5	1.5	48,000	9.3	0.345	n.a.	n.a.	23	n.a.	[27]
2	Fe@ZrO_2–10	220	5	2	48,000	8	0.251	1	19	35	65	[26]
3	$Cu_{5.2}Fe_{4.8}$	350	5.5	2.0	6000 h^{-1}	71	0.177	18	18	12	n.a.	[19]
4	3Cu17FeCoK/ Attapulgite	225	3	1.0	2000	10	0.118	6.4	10	54[b]	40	This work
5	Ca-Fe	190	4	2.0	4800	11	0.072	6[a]	5[a]	47[a]	44[a]	[28]
6	0.7Ru-CoMn	220	6	1	2000	32	0.047	23	5	31	23	[29]
7	CuCoAl/ZnO/ZrO_2	250	5	2.0	4000	13	0.033	19[a]	15[a]	42[a]	40[a]	[25]
8	Ca-Fe	190	4	2.0	4800	11	0.072	6[a]	5[a]	47[a]	44[a]	[28]
9	CuFe/SiO_2	250	5	2.5	3000 h^{-1}	42	n.a.	18	n.a.	22	60	[24]

[a] wt%.
[b] Liquid products.

Table 3
Alpha, modified alpha, R^2, beta values and water concentration (wt-%) for the tested catalysts at different reaction temperatures and H_2:CO ratios.

Catalyst	Temperature (°C)	H_2:CO	α	R^2	β	H2O	α'	$R^{2'}$
12Cu8FeCoK/attapulgite	225	2	0.29	0.96	1.27	n.a.	0.29	0.94
	250	2	0.28	0.99	1.78	69.1	0.27	0.99
	275	2	0.29	0.99	1.83	72.5	0.27	0.99
	300	2	0.31	0.98	2.78	84.8	0.29	0.98
	225	1	0.44	0.93	2.72	99.1	0.45	0.90
	250	1	0.29	0.98	1.90	81.3	0.28	0.97
	275	1	0.29	0.99	1.97	73.9	0.27	1.00
	300	1	0.28	0.97	2.84	76.2	0.27	0.97
3Cu17FeCoK/attapulgite	225	2	0.32	0.96	2.02	78.1	0.31	0.95
	250	2	0.27	0.99	1.98	74.0	0.26	0.99
	275	2	0.30	0.97	2.61	81.8	0.29	0.96
	300	2	0.35	0.95	3.61	90.3	0.33	0.94
	225	1	0.37	0.96	2.37	93.6	0.36	0.95
	250	1	0.31	0.97	2.20	84.3	0.31	0.97
	275	1	0.29	0.97	2.50	78.3	0.28	0.97
	300	1	0.33	0.94	3.28	85.2	0.32	0.93
17Cu3FeCoK/attapulgtie	225	2	0.47	0.87	1.09	95.5	0.52	0.83
	250	2	0.32	0.93	1.42	80.5	0.32	0.90
	275	2	0.33	1.00	1.60	68.2	0.32	1.00
	300	2	0.30	0.99	1.67	78.4	0.30	0.98
	225	1	0.41	0.93	1.88	94.3	0.42	0.91
	250	1	0.35	0.97	1.45	90.1	0.36	0.95
	275	1	0.30	1.00	1.79	68.6	0.29	1.00
	300	1	0.29	1.00	1.74	70.2	0.28	1.00

for CO_2, n-alkanes ranging from methane to hexane and linear α-olefins ranging from ethene to hexene.

The collected liquid product was analyzed by GC (HP 6890 Series). Separation of the alcohols was done in a FFAP column using the following temperature program, 2 min at 50 °C, heating to 220 °C with 5 °C/min and holding for 10 min. The flame ionization detector was calibrated for linear primary alcohols starting from methanol all the way up to 1-decanol.

The water concentration in the collected liquid samples was quantified by Karl Fischer titration in dry methanol (Fluka) using Hydranal Composite 2 (Fluka) as the titrant.

The coke content on the catalysts was determined by thermal gravimetric analysis (TGA) using a Discovery SDT 650 instrument. The analysis was carried out in a 100 mL/min flow of air with a 10 °C/min heating rate up to 800 °C. A 90 μL alumina cup was used to hold the spent catalyst sample (10–35 mg).

2.2.8. Calculations

The volumetric flow of the eluting gases was calculated based on the known flow of nitrogen used as the internal standard and the calibrated responses of the TC and FI detectors.

The conversion of CO was calculated according to

$$X_{CO,i} = 1 - \frac{\dot{V}_{CO,i}}{\dot{V}_{CO,0}} \quad (1)$$

Where $\dot{V}_{CO,0}$ is the flow of CO entering the reactor and $\dot{V}_{CO,i}$ is calculated flow of eluted CO.

The calculation of hydrogen conversion was done taking into account a possibility of the water gas shift reaction (WGSR), forming additional hydrogen

$$X_{H2,i} = 1 - \frac{\dot{V}_{H2,i} - \dot{V}_{CO2,i}}{\dot{V}_{H2,0}} \quad (2)$$

Where $\dot{V}_{H2,0}$ is the volumetric flow of hydrogen entering the reactor and $\dot{V}_{H2,i}$ is the calculated flow of outgoing hydrogen. The outgoing flow of carbon dioxide $\dot{V}_{CO2,i}$ was subtracted from the flow of the detected hydrogen because additional hydrogen was formed during possible WGSR.

Selectivity to different gas phase products is calculated with the equation

$$S_{x,i} = \frac{n_x \bullet \dot{V}_{x,i}}{\dot{V}_{CO,0} - \dot{V}_{CO,i}} \quad (3)$$

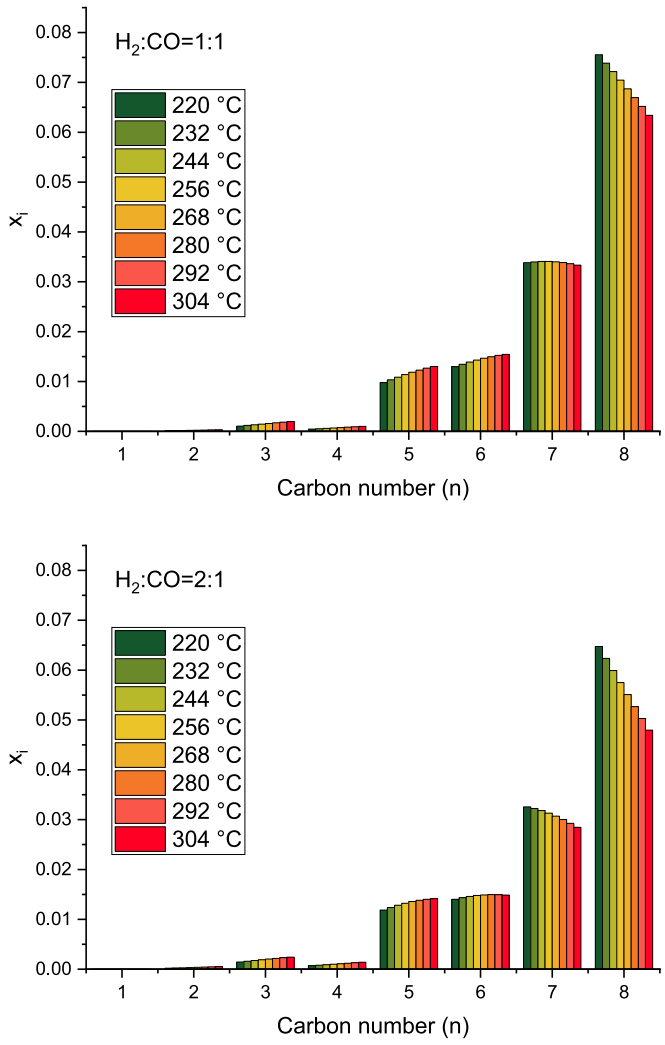

Fig. 10. Molar fraction of linear alcohols calculated using the Gibbs reactor module implemented in ChemCAD software.

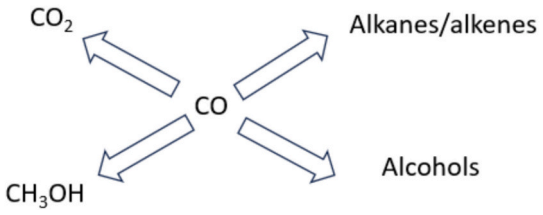

Scheme 1. A simplified reaction network.

Where n_x is the number of carbon atoms in the product x and $\dot{V}_{x,i}$ is the volumetric flow of the product. The denominator is the converted flow of CO. Selectivity to the liquid products is calculated through a difference from selectivity of the gas phase products. Possible coke formation is not taken into account in the equations above.

Based on Eq. (2) and (3) the yields can be calculated based on hydrogen conversion.

The chain growth probability (α) is calculated with the Anderson-Schulz-Flory (ASF) distribution shown in Eq. (4).

$$\frac{W_n}{n} = (1-\alpha)^2\alpha^{n-1} \quad (4)$$

Table 4
Values of apparent activation energies.

		CO insertion			CHn formation
Catalyst	H_2:CO	E_act	ln A	E_act	ln A
3Cu17FeCoK	2	68	23	89	29
	1	71	23	102	31
12Cu8FeCoK	2	53	19	91	29
	1	43	16	111	32
17Cu3FeCoK	2	84	25	107	31
	1	31	13	121	34

Where W_n is the weight fraction of the product (alcohol, alkane or alkene) with n number of carbon atoms.

As shown later in the paper the α-values for the alcohols formed over the different catalysts are rather similar. Therefore another descriptor, β, had to be introduced. The eq. (5) gives the ratio of the desired higher alcohols (C_{2+}) in relation to methanol.

$$\beta = \frac{1 - W_{MeOH}}{W_{MeOH}} \quad (5)$$

Where W_{MeOH} is the weight fraction of methanol.

3. Results and discussion

3.1. Catalytic results

A typical plot of the volumetric flows of CO, H_2 and N_2 is shown in Fig. 2 using the 12Cu8FeCoK/attapulgite catalyst as an example.

Four different temperatures are used in Fig. 2, namely 225, 250, 275 and 300 °C showing how the values of flow of both hydrogen and CO decreases when the reaction temperature is increased, i.e. conversion of both CO and H_2 increases. The values for conversions and selectivity will be presented below. Two different H_2:CO ratios are used, namely 2 in the left part of the graph and 1 in the right side.

The time-on-stream plot for the volumetric flow of the produced alkanes and CO_2 is shown in Fig. 3 over the same 12Cu8FeCoK/attapulgite as presented above.

From Fig. 3 it can be observed that the main products, in terms of volumetric flow, are methane and CO_2, followed by significantly lower flows of ethane, propane, etc. Some catalyst deactivation can be seen in Fig. 2 and Fig. 3 as the flow of CO increases slightly at 250 and 275 °C with H_2:CO equal to 2 and vice versa the flows of methane and CO_2 decreased at these temperatures. Otherwise, the catalyst demonstrated a rather stable behavior.

The flows of alkenes are shown in Fig. 4.

Interesting trends can be observed in Fig. 4, namely the flows of alkenes seem to decrease with increasing temperature when the gas feed H_2:CO ratio is 2, except 225 and 250 °C, while at the lower H_2:CO ratio the flows increase with temperature. Compared to the flows of alkanes and CO_2 the flows of alkenes are significantly lower.

The flows of CO, H_2, alkanes and alkenes shown in Fig. 2 - Fig. 4 were used to calculate the conversion of CO and H_2 as well as selectivity to alkenes, alkanes and CO_2 which are listed in Table 1 for all three catalysts evaluated in this work.

Gong et al. [24] studied stabilizing strategies for CuFe/SiO_2 catalysts with or without piranha solution treatment. The aimed Cu:Fe ratio of their catalyst was 1:1 which can be compared with our 12Cu8FeCoK catalyst, however, the nominal metal loading on their catalyst was reported to be 0.03 mol per 10 g support, which corresponds to roughly 11 wt-%. In their catalyst evaluation experiments they used only one reaction temperature (250 °C) and slightly higher pressure (5 MPa), GHSV ($3000h^{-1}$) and H_2:CO (2.5). In any case some comparison with the current work can be done. Gong et al. [24] reported an initial CO conversion of ca. 40%, which is in agreement with our results at 250 °C.

Table 5
TGA results.

Catalyst	weightloss (%)	Onset T (°C)	weight increase (%)	Onset T (°C)	weightloss (%)	Onset T (°C)	weightloss (%)	Onset T (°C)	Heat of weight loss/ increase (J/g)	coke amount (wt-%)
17Cu3FeCoK (fresh)	2.8	47	2.3	140	–	–	1.3	440	195 (201 °C)	–
17Cu3FeCoK (spent)	3.7	34	0.1	270	3.3	331	–	–	72 (340 °C)	5.1
12Cu8FeCoK (fresh)	1.3	35	3.0	130	–	–	1.7	340	284 (157 °C)	–
12Cu8FeCoK (spent)	2.5	33	0.2	160	1.4	224	6.6	335	341 (258 °C), 104 (347 °C)	10.5
3Cu17FeCoK (fresh)	1.9	59	3.0	125	–	–	2.2	310	519 (182 °C)	–
3Cu17FeCoK (spent)	1.6	54	0.5	177	14.8	304	–	–	1912 (323 °C)	14.4

Selectivity to alkanes and alkenes, CO_2 and higher alcohols are also comparable, as a combined alkane+alkene selectivity of approximately 60%, CO_2 selectivity of 25% and selectivity to higher alcohols just below 20% was reported [24]. The rates of CO and hydrogen conversion in μmol g_{cat}^{-1} s^{-1} are plotted as a function of temperature for different catalysts in Fig. 5.

From Fig. 5 it can be observed that a higher iron loading at the expense of copper elevated conversion of both CO and hydrogen. Moreover, a higher H_2:CO ratio improves conversion, except for CO transformation rates with 3Cu17FeCoK and 12Cu8FeCoK catalysts at the highest reaction temperatures, which is due to almost complete conversion of CO at 300 °C for these catalysts as listed in Table 1. Similarly, the hydrogen reaction rate (Fig. 5b) is increased with temperature and the H_2:CO ratio. Interestingly, for 3Cu17FeCoK and 12Cu8FeCoK the conversion of hydrogen exceeded 100% (Table 1) at the highest temperature. As no additional hydrogen can be generated by other reactions, such as the water gas shift requiring water formed as well from hydrogen, the values exceeding 100% conversion should be attributed to analysis/calibration errors.

Gong et al. [24] reported an initial CO conversion level of ca. 40%, as mentioned above, which should correspond to the CO reaction rate of 4.2 μmol g_{cat}^{-1} s^{-1}, higher than obtained here. A possible reason can be a higher H_2:CO ratio (2.5:1) than in the current work, as the reaction rate is increasing with a higher H_2:CO ratio.

Based on the results presented above the apparent activation energy for CO conversion was calculated to be 78, 80 and 90 kJ/mol for the 3Cu17FeCoK, 12Cu8FeCoK and 17Cu3FeCoK catalysts, respectively, at H_2:CO = 2. The activation energy at the lower H_2:CO ratio was 86, 79 and 74 kJ/mol. Changes in activation energy at different conditions are an indication of a complex reaction mechanism with several steps like CHx generation and CO insertion contributing to the overall rate. Interestingly, that most changes were visible for 17Cu3FeCoK catalyst. More detailed kinetic analysis is planned to explore the impact of reaction conditions in a quantitative way.

Guo et al. [19] reported that by increasing the iron content of the catalyst the conversion of CO increased, which is in line with our results (Table *1*), however, significantly higher temperature (350 °C), pressure (55 bar) and GHSV (6000 h^{-1}) were used compared to our reaction conditions. Zeng et al. [3] used bimetallic Au—Fe and monometallic gold and iron catalysts in their research on HAS, reporting that CO conversion decreased with an increasing gold content due to a partial coverage of iron carbides, as iron species were considered responsible for CO dissociation.

The main products in the gas phase were methane and CO_2, with selectivity to these products as a function of CO conversion displayed in Fig. 6.

In Fig. 6a clear differences between the catalysts and H_2:CO ratio can be observed for the methane selectivity. A higher copper content in the catalyst and a higher H_2:CO ratio yields more methane, similar to the study of Guo et al. [19] when the highest methane selectivity was obtained with the copper rich catalyst. A feed gas containing more hydrogen, i.e. a higher H_2:CO ratio, as observed in the Fig. 6a generated more methane because for 1 mol of methane 3 mol of hydrogen are required. No clear differences between the catalysts or H_2:CO ratio can be observed for CO_2 selectivity (Fig. 6b), i.e. the Cu:Fe ratio has no impact on the CO_2 selectivity at similar CO conversion levels. Comparison with the study of Guo et al. [19], who used similar CuFeCo/attapulgite catalysts with different Cu:Fe ratios, is not straightforward as only one temperature was tested by Guo et al. [19]. However, the copper rich catalyst displayed a significantly lower CO conversion and CO_2 selectivity than the other catalysts that had conversion levels of ca. 70% and CO_2 selectivity of 20%, which are slightly lower than the results presented in Fig. 6.

While the main aim of the study was to obtain higher alcohols, the authors consider it very instructive to elucidate selectivity not only to them and carbon dioxide, but also to hydrocarbons. The combined selectivity for alkanes and alkenes, is plotted against the CO conversion in Fig. 7 for the tested catalysts.

The opposite trends can be seen in Fig. 7a, selectivity to alkanes increases with CO conversion, i.e. at higher reaction temperature, while selectivity to alkenes (Fig. 7b) decreases with CO conversion. A possible reason for the differences could be enhancement of WGSR at higher temperature giving thus more hydrogen which can hydrogenate alkenes to alkanes. The 3Cu17FeCoK catalyst exhibited the lowest selectivity to alkanes giving the highest to alkenes, contrary to the 17Cu3FeCoK catalyst. Formation of alkenes can be considered desirable in the context of higher alcohols synthesis because they can be hydrated to alcohols. Moreover, as the alkenes have a carbon number 2 or higher, therefore, all alcohols formed during hydration can be regarded as higher alcohols.

Selectivity to the liquid products, calculated by the difference, is presented as a function of CO conversion for the different catalysts and H_2:CO ratios in Fig. 8.

From Fig. 8 it can be observed that selectivity to the liquid products decreases with increasing 4H2 and CO and in the presence of surface Fe2C2-Fe2Osimilar CO conversion.

The collected liquid was analyzed for the alcohol content using GC. The weight fraction of different alcohols detected in the liquid samples is shown in Fig. 9.

As a comparison the performance of different catalysts in syngas transformation to alcohols is shown in Table 2 [19,24–29]. Typically higher alcohol synthesis has been performed under 3–6 MPa in the temperature range of 190–250 °C with some exceptions utilizing a higher temperature [19]. The highest space-time yield (STY) of alcohols was reported over Co_1Fe_4@ZrO_2–10 in which highly dispersed metal oxides were present. This catalyst was also very stable for 300 h [27]. The second highest STY yield for alcohols was obtained over Fe@ZrO_2–10, in which ZrO_2 was able to activate H_2 and CO and moreover the Fe_2C_2-Fe_3O_4 interfacial sites were suggested to be catalytically active. In addition, bimetallic $Cu_{5.2}Fe_{4.8}$ was also very productive towards higher alcohols even at a higher temperature [19]. As

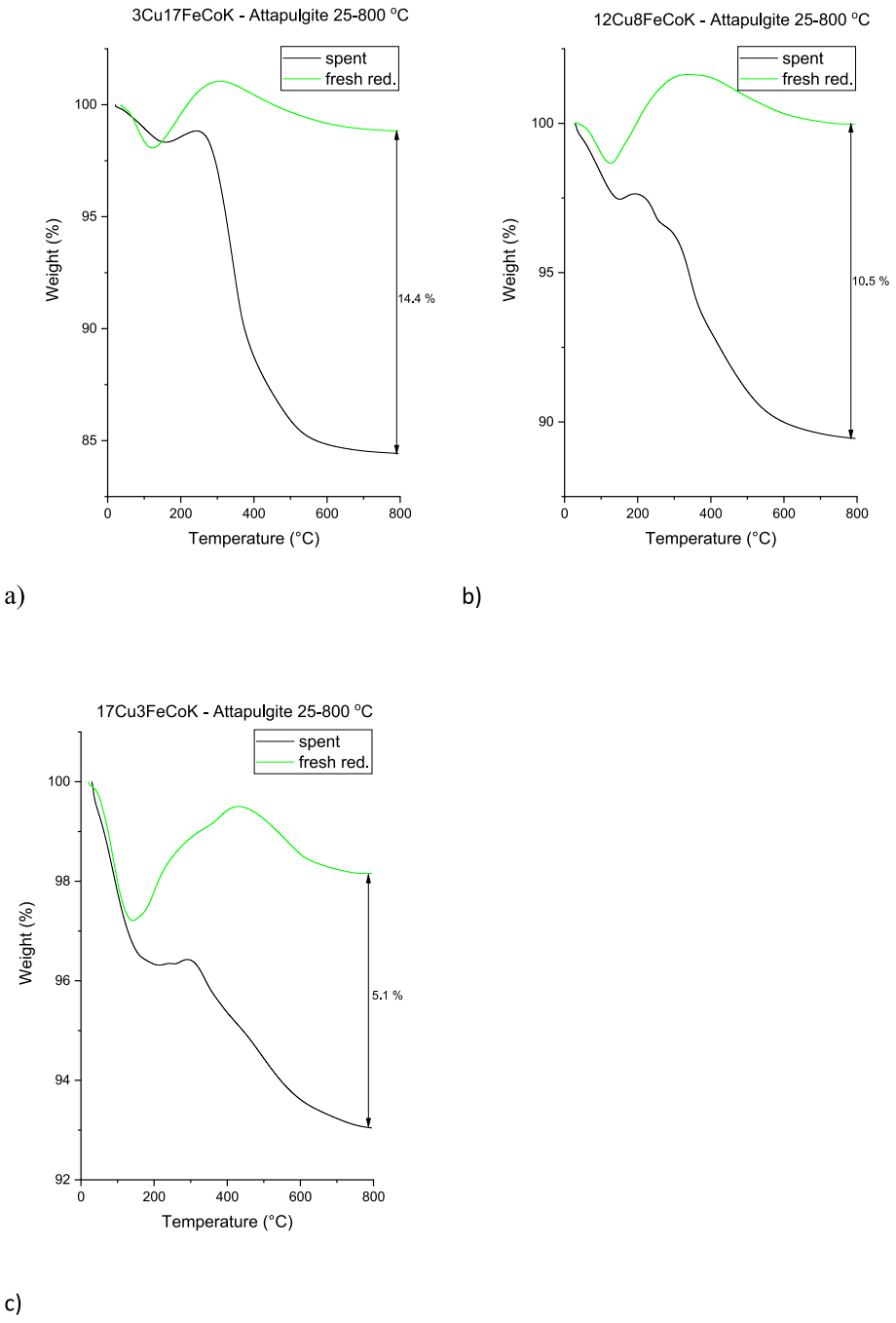

Fig. 11. Normalized coke weight loss curves for the studied catalysts a) 12Cu8FeCoK, b) 3Cu17FeCoK, c) 3Cu17FeCoK.

can be seen from Table 2, the performance of 3Cu17FeCoK/Attapulgite is very good, giving a high STY and low selectivity to CO_2 and methane. It has been reported that methane formation was suppressed over potassium modified Cu-Fe/SiO_2 catalyst, while in the absence of potassium the methane selectivity was nearly 1.5 fold higher [30]. It can also be seen that the H_2/CO ratio typically varies in the range of 1–2.5 in syngas transformation to higher alcohols. Analogously to the current results with H_2/CO ratio of 1 promoting higher alcohol formation, an optimum H_2/CO ratio of 1 gave the highest selectivity to alcohols in [29] over 0.7Ru-CoMn catalyst. Furthermore, an optimum H_2/CO ratio of 1.5 resulted in the highest space time yield of alcohols over Fe@ZrO_2–10 catalyst [26].

From the results shown in Fig. 9 for alcohols it is possible to calculate the α- and β-values, which are listed in Table along with the coefficient of determination, R^2, of the linear fit for the α-value defined by eq. (4). According to Table 3, the α-values are more or less similar for the three different catalysts tested independent on the reaction temperature and the H_2:CO ratio.

The average α-value for the 12Cu8FeCoK/attapulgite is 0.31. The highest values of α are, however, calculated with the lowest values of R^2. This can be seen as an indication that the alcohol distribution for these cases is not following closely the Anderson-Schulz-Flory distribution. Besides 12Cu8FeCoK catalyst, the same observations can be made for some of the α-values and R^2-values with the copper rich (17Cu3FeCoK/attapulgite) catalyst. The average α-values for 3Cu17FeCoK/attapulgite and 17Cu3FeCoK/attapulgite are 0.32 and 0.35, respectively. Based on α-values no clear differences can be observed for the performance of different catalysts.

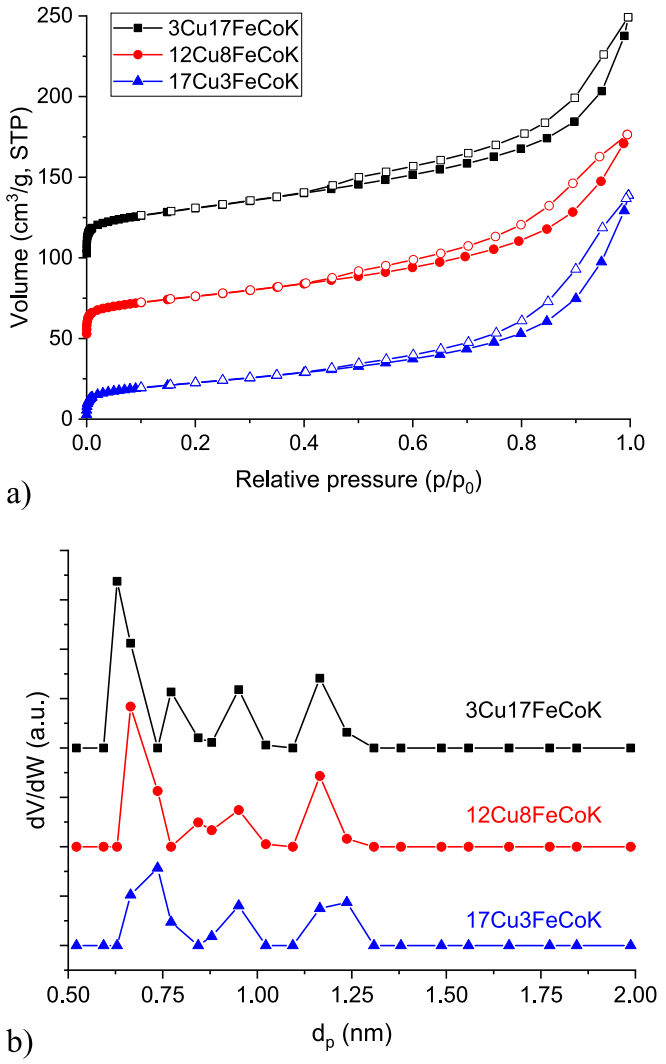

Fig. 12. Textural properties characterization: a) nitrogen adsorption isotherms for different catalysts with closed and open symbols representing respectively adsorption and desorption, b) micropore size distribution.

Table 6
Specific surface area, pore volume (V_p), micropore volume (V_{micro}) and mesopore volume (V_{meso}) of fresh catalysts and spent (in parenthesis).

Catalyst	BET area (m^2/g)	V_p (cm^3/g)	V_{micro} (cm^3/g)	V_{meso} (cm^3/g)
3Cu17FeCoK	110 (7)	0.19 (0.00)	0.03 (0.00)	0.16 (0.00)
12Cu8FeCoK	93 (33)	0.17 (0.01)	0.03 (0.00)	0.15 (0.01)
17Cu3FeCoK	79 (48)	0.18 (0.02)	0.02 (0.00)	0.16 (0.02)

However, the average β-values (1.58, 2.14 and 2.57) give a clear trend namely that the lowest β-value corresponds to the copper rich, 17Cu3FeCoK/attapulgite, catalyst while the copper poor catalyst, 3Cu17FeCoK/attapulgite exhibited the highest β-value, indicating formation of more of the desired higher alcohols. The trend of β-values correspond well to previously reported trends, namely higher copper content catalysts generates less of higher alcohols [19], with the ratio of higher alcohols to methanol between 0.79 and 1.67. The liquid samples contained a significant amount of water, which can be expected, as water is formed in most of the reactions taking place except methanol formation and the WGSR, where it is even consumed. Gong et al. [24] for a catalyst with 1:1 Cu:Fe ratio supported on SiO_2 observed methanol selectivity of initially just below 70% and decreased with time to below 60% after 92.5 h. 60% - 70% methanol selectivity corresponds to

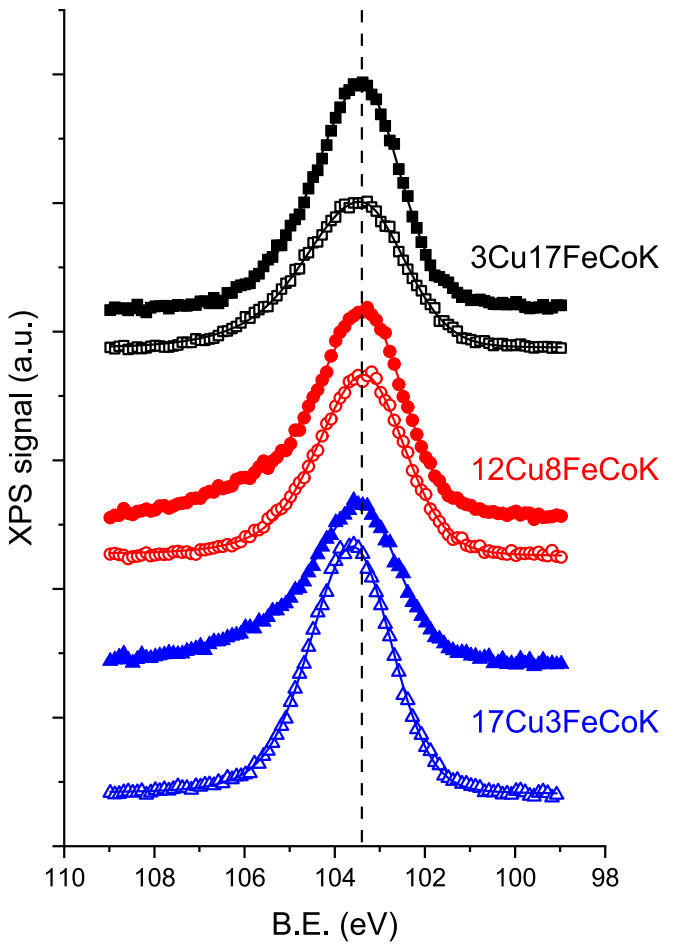

Fig. 13. Si 2p spectra for as prepared (closed symbols) and spent (open symbols) for different catalysts.

β-values of 0.42 to 0.67, which are significantly lower than obtained in the current work (Table). A possible reason for lower β-values in [24] is utilization of a bi-metallic CuFe catalyst, while in this work cobalt and potassium are used as additives besides copper and iron.

The equilibrium composition was computed using the Gibbs reactor module implemented in ChemCAD software [31]. The non-ideality of the system was taken into account adopting the PSRK equation of state, as suggested in the literature [2]. The computations were conducted fixing a total pressure in a range of 1–100 bars, in a temperature range between 100 and 400 °C, and a feed composition of 1:1 and 2:1 CO to H_2. Only linear alcohols were considered.

The molar fraction of gas phase products excluding alkanes and alkenes for the linear alcohols for the different H2:CO ratios at the temperature range used in this work are plotted in Fig. 10 presented below.

Based on the results presented above one can conclude that our results are limited by kinetics as our experimental results shows a distribution of alcohols in an opposite trend.

Calculations of the α-values above are based on hypothesis that the alcohol distribution is following the Anderson-Schulz-Flory treatment. A more realistic picture is given in Scheme 1, where formation of methanol is decoupled from generation of other alcohols.

This approach is based on a concept that chain growth happens through generation (CHn)x monomers, which are either hydrogenated to alkane/alkene or undergo CO insertion followed by hydrogenation into the alcohol product. Formation of methanol is thus different originating from hydrogenation of CO. The modified values of the α-values above, which do not take into account methanol in the distribution of alcohols, are given in Table along with the corresponding values of (R^2)'

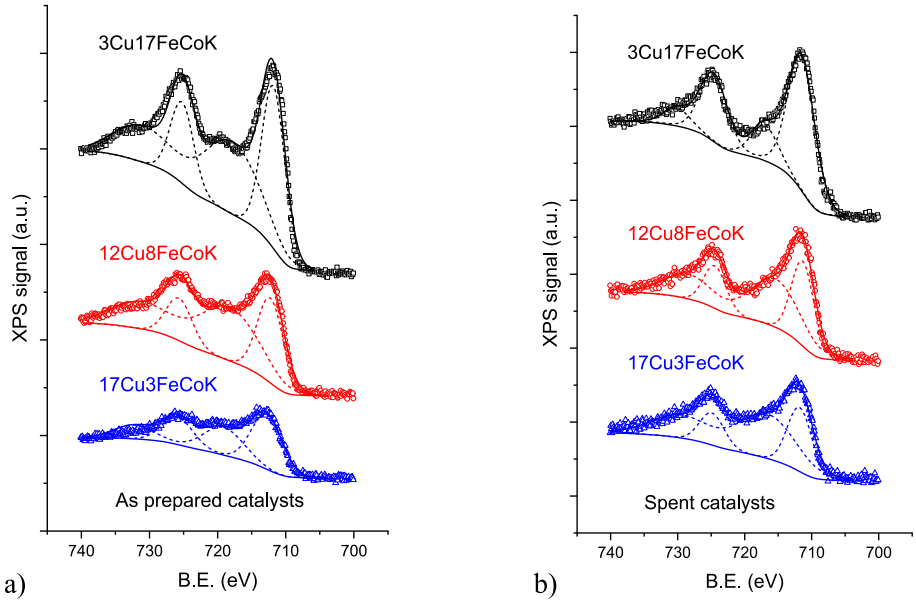

Fig. 14. Fe 2p spectra for the fresh (a) and spent (b) catalysts with different Cu:Fe ratios.

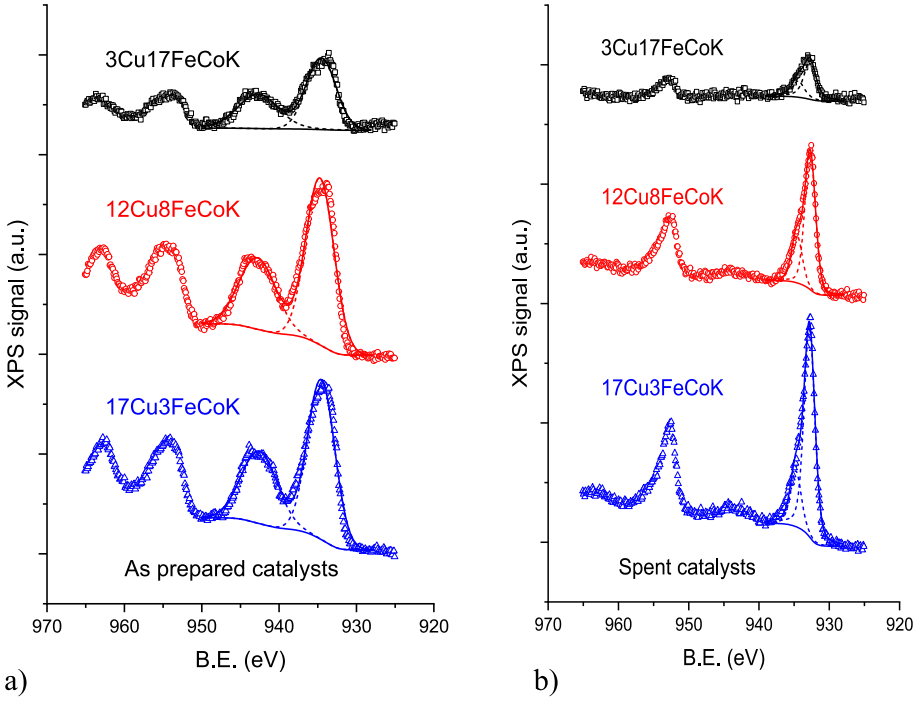

Fig. 15. Cu 2p spectra for fresh (a) and spent (b) catalysts with different Cu:Fe ratios.

values indicating similar description of the experimental data.

It should be also noted that the Anderson-Schulz-Flory distribution assumes that the chain growth probability does not change with the carbon number, and thus the ratio of hydrogenation vs CO insertion constants for (CHn)x intermediates is the same independent on the carbon number. In the current work deviations were clearly seen at a relatively high chain length (carbon number of 7–10), indicating that the idealized chain growth probability is not applicable for the case of synthesis of higher alcohols. In fact, deviations from the ideal ASF distribution have been reported also for longer-chain (C_{10+}) hydrocarbons [32].

While detailed kinetic modelling is required to quantify the product distribution, a rather simple analysis can be done for H termination and CHn coupling reactions just based on respective selectivity values assuming that the activation energy is independent of chain length.

The descriptors for the yields of alcohols and hydrocarbons were defined as

$$y_{CO,n} = \frac{S_{C_n alcohol}}{n} \frac{S_{liquid}}{\sum S_{C_i alcohol}/i} \frac{X_{CO}}{(1 - S_{CO2} - S_{MeOH})} \quad (6)$$

$$y_{CH,n} = \frac{S_{C_n HC}}{n} \frac{(1 - S_{liquid})}{\sum S_{C_i HC}/i} \frac{X_{CO}}{(1 - S_{CO2} - S_{MeOH})} \quad (7)$$

where i and n are carbon numbers and “HC” includes both alkanes and alkenes.

Table 7
XPS peak positions (eV) of Fe2$p_{3/2}$ and Cu2$p_{3/2}$ for the different as prepared and spent catalysts.

Catalyst		Fe $2p_{3/2}$	Fe_{SA}	Cu $2p_{3/2}$ 1	$Cu2p_{3/2}$ 2	Cu_{SA}
3Cu17FeCoK	fresh	711.8	717.9	934.6 (100.0%)	n.a.	942.8
	spent	711.5	717.0	934.4 (29.8%)	932.8 (70.2%)	n.a.
12Cu8FeCoK	fresh	712.3	718.2	934.7 (100.0%)	n.a.	942.8
	spent	711.3	715.4	934.6 (25.9%)	932.7 (74.1%)	n.a.
17Cu3FeCoK	fresh	712.8	719.1	934.6 (100.0%)	n.a.	942.6
	spent	711.8	716.6	934.8 (20.9%)	932.8 (79.1%)	n.a.

The apparent activation energies were calculated for these descriptors and presented in Table 4 for the hydrogen to CO ratio of.

For CHn formation the activation energy increased with higher copper (and subsequently lower Fe) content while for CO insertion activation energy behavior was dependent on the hydrogen to CO ratio. For H_2:CO equal to unity, an increase of Fe content increased the activation energy, while with this ratio equal to 2 a minimum at moderate Fe content was observed pointing out that the optimal conditions for CO insertion may depend on the Cu:Fe ratio.

The Cu-rich 17Cu3FeCoK catalyst at H_2:CO = 1 was found to exhibit the highest selectivity towards the liquid products, which is in line with lowest activation energy of 31 kJ/mol for CO insertion. The CO insertion barrier is highly dependent on the H_2:CO ratio, increasing to 84 kJ/mol at H_2:CO = 2, with a corresponding major increase in the pre-exponential factor. If such behavior is not related to an apparent compensation effect, then such variation could in general indicate a change in the alcohol synthesis mechanism under these conditions.

The coke content of the samples determined by TGA are listed in Table 5 and the normalized weight loss curves in Fig. 11.

3.2. Catalyst characterization results

3.2.1. N_2-physisorption results

The nitrogen isotherms for different catalysts are displayed in Fig. 12. The isotherms for 3Cu17FeCoK and 12Cu8FeCoK have been increased (shifted along Y axis in Fig. 12 for better visual representation of the isotherms) with 100 and 50 cm^3/g, respectively.

The specific surface areas of the fresh and spent (in parenthesis) catalysts, calculated with the BET equation, are listed in Table 6. From the results presented in this table, it is noticed that the specific surface area and the amount of micropores smaller than 1 nm, decreased with the increasing copper content. Guo et al. [19] used similar catalysts in their work and found that the catalyst with the highest iron content possessed the highest surface area then the support material (attapulgite).

A significant decrease in the specific surface area and pore volume can be observed for the spent catalysts. A possible reason could be that after the experiments the heating of the reactor was discontinued while keeping the flow of syngas and thereby reaction products adsorbed to the surface could not desorb, or that coke deposits were formed on the catalyst surface blocking the pores. However, the catalysts were outgassed at 180 °C overnight and for 4 h at 250 °C prior to the N_2-physisorption. Interestingly, the "high" surface area 3Cu17FeCoK catalyst showed the largest decrease, from 110 to 7 m^2/g. in surface area and vice versa for the "low" surface area 17Cu3FeCoK catalyst.

3.2.2. XPS results

Possible charging of the catalyst sample was investigated by using the Si2p peak as a reference, with the raw data shown in Fig. 13 for the fresh and spent catalysts.

No significant sample charging can be seen in Fig. 13 as all peaks have the maximum at approximately 103.5 eV, typical for Si 2p of SiO_2 which should be present in attapulgite used as the support material. However, some peak broadening is visible for the fresh (as prepared) and spent 3Cu17FeCoK, and fresh 12Cu8FeCoK and 17Cu3FeCoK materials compared to the spent samples of these catalysts. A possible reason for peak broadening is a fairly large size of catalyst particles (125–250 μm), whereas some crushing might occur during catalyst

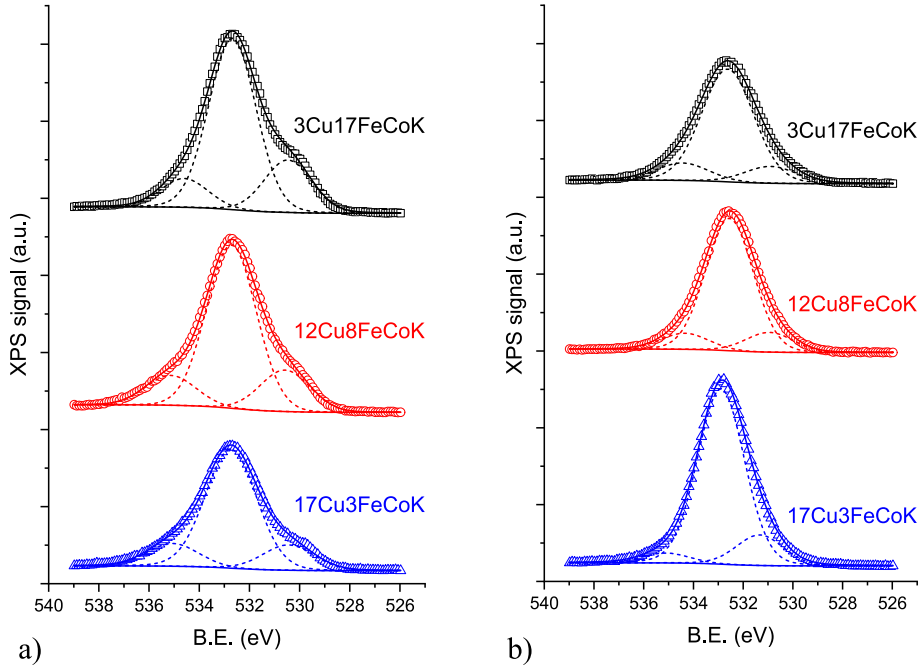

Fig. 16. O 1 s spectra for fresh (a) and spent (b) catalysts with different Cu:Fe ratios.

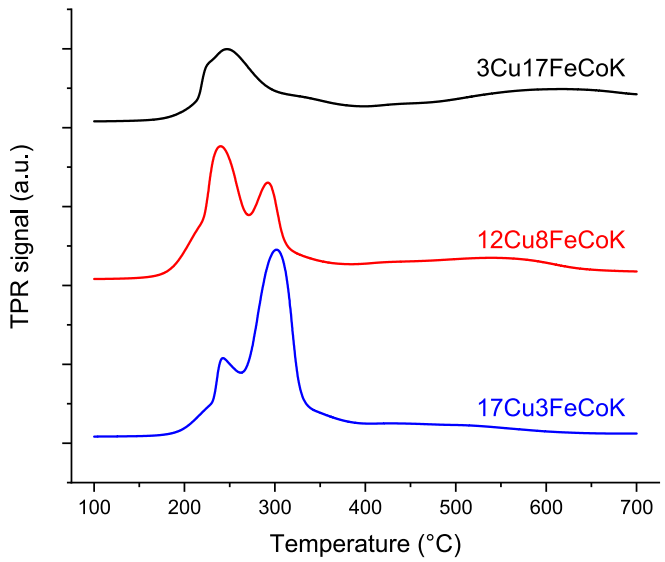

Fig. 17. TPR curves for fresh catalysts.

removal from the reactor.

The Fe 2p spectra are displayed in Fig. 14, while the data for Cu 2p are illustrated in Fig. 15 showing the Shirley background and peak fitting of the data. The peak positions of Fe $2p_{3/2}$ and Cu $2p_{3/2}$ are listed in Table 7 along with the ratio between different Cu peaks.

No major differences between the fresh and spent Fe $2p_{3/2}$ peak can be observed in Fig. 14, however, the peak position is at slightly lower binding energies for the spent samples compared to the fresh ones. The Cu 2p spectra of the fresh and spent samples show clear differences as the satellite peaks are absent in the spent samples. The peak position of Fe $2p_{3/2}$ corresponds fairly well to Fe^{+3} (Fe_2O_3) as reported by [24,33,34]. For the Cu 2p the peak positions and the presence or absence of the satellite peak indicate according to Biesinger et al. [35] that copper in the fresh samples is either in the form of CuO or $Cu(OH)_2$ and in the spent samples is reduced to Cu^0 with a lower contribution of CuO. Combining the XPS results for copper and iron could indicate that these metals might exists as $CuFe_2O_4$ cuprospinel, the possible existence of this phase is investigated by XRD and discussed below.

The O 1 s spectra for fresh and spent catalysts with the peak fitting is shown in Fig. 16.

A clear shoulder can be seen for the fresh samples on the right side of the spectra because of metal oxides (530.8 eV) and SiO_2 (532.7 eV) as reported by [36]. The shoulder is not as pronounced for the spent samples and could be seen as an indication that the spent catalyst samples contain a lower concentration of metal (Cu) oxides.

In this work the fresh catalysts were exposed to CO to stabilize them following the procedure from the literature for various iron-based Fischer-Tropsch catalysts, where such exposure typically results in formation of iron carbide. Based on XPS results no formation of iron carbide visible at 702.1 eV [37] was noticed. In fact, introduction of Co and Cu in the catalyst composition in certain amounts prevents iron carbide formation. For example, carburization with ethylene occurred for Fe/$CaCO_3$ [38], being absent for Fe-Co/$CaCO_3$.

3.2.3. TPR results

Temperature programmed reduction was carried out on the 3 different catalysts and the results are shown in Fig. 17.

Fig. 17 clearly illustrates different reduction behavior of the three catalysts. For the copper rich catalysts 12Cu8FeCoK and 17Cu3FeCoK catalysts two reduction peaks at 300 °C and 250 °C can be seen while for the copper poor 3Cu17FeCoK catalyst only one at the lower temperature. A possible reason for the differences in the TPR curves could be as reported by He et al. [39] that the peak at 250 °C is due to reduction of highly dispersed CuO species while the peak at 300 °C is due to reduction "bulk" CuO, their findings were in agreement with XRD results. The reduction of Fe is not as pronounced as the reduction of Cu in Fig. 17 and should occur at temperatures above 400 °C according to [40]. Furthermore, reduction of the attapulgite support, which occurs at 650 °C [41] was not visible in the current work.

3.2.4. XRD

Powder X-ray diffraction patterns of fresh 17Cu3FeCoK, 12Cu8FeCoK and 3Cu17FeCoK samples obtained after calcination and reduction are presented in Fig. 18. These patterns were obtained on a diffractometer configured with a molybdenum X-ray diffraction source providing X-rays with a wavelength of 0.7093 instead of Cu X-ray diffraction source (λ = 1.5418 Å) to avoid undesirable fluorescence effect of Cu, Fe and Co. It was shown all XRD patterns contain reflexes from the palygorskite (PDF No. 00–031-0783) and SiO_2 (quartz) (PDF# 00–046-1045). The 17Cu3FeCoK catalyst contains reflexes from Cu^0 (PDF № 00–004-0836, a = b = c = 3.615 Å) with the determined value of the lattice parameter a = b = c = 3.615(1) Å and the average coherently scattering domain (CSD) size D_{Cu} = 30.5 nm. 12Cu8FeCoK also contains reflexes from Cu^0 (PDF № 00–004-0836, a = b = c = 3.615 Å) with the value of the lattice parameter a = b = c = 3.616(1) Å and a similar average CSD size D_{Cu} = 30 nm. Both Cu-enriched samples 17Cu3FeCoK and 12Cu8FeCoK contain highly dispersed crystal phase of

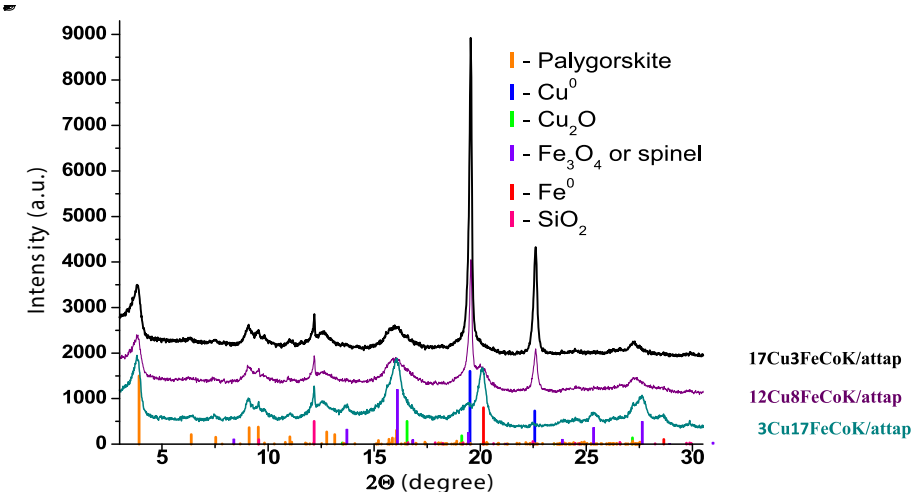

Fig. 18. XRD patterns of calcined reduced 17Cu3FeCoK, 12Cu8FeCoK and 3Cu17FeCoK catalysts before the reaction.

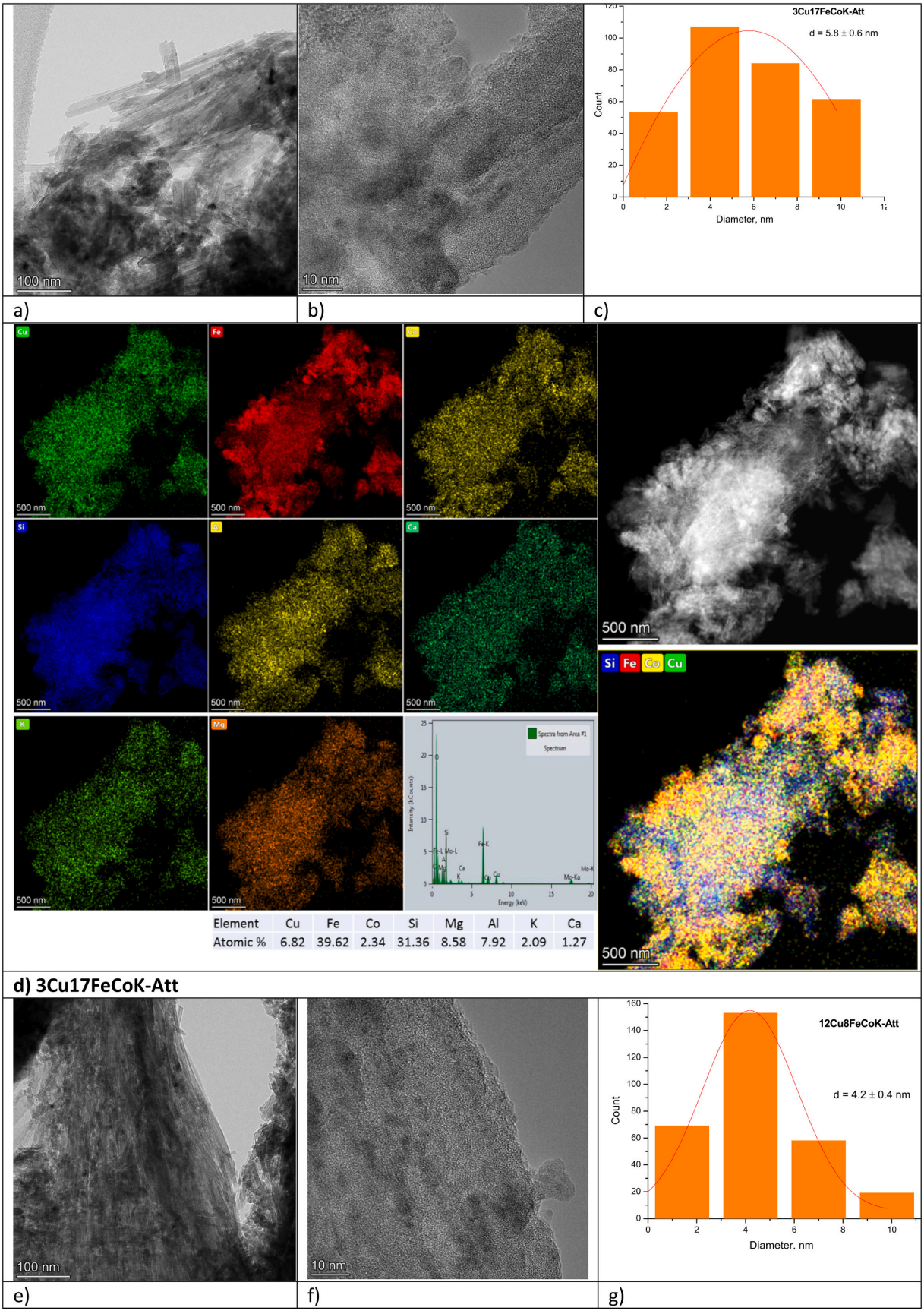

Fig. 19. TEM, HAADF-STEM images and EDX elemental mapping of reduced fresh catalysts: a-d) 3Cu17FeCoK-Att, e-h) 12Cu8FeCoK-Att, i-l) 17Cu3FeCoK-Att. Fe (red), Co (yellow), Cu (green), Mg (orange), Al (dark yellow), Si (blue), K (grassy green), Ca (dark green). (For interpretation of the references to colour in this figure legend, the reader is referred to the web version of this article.)

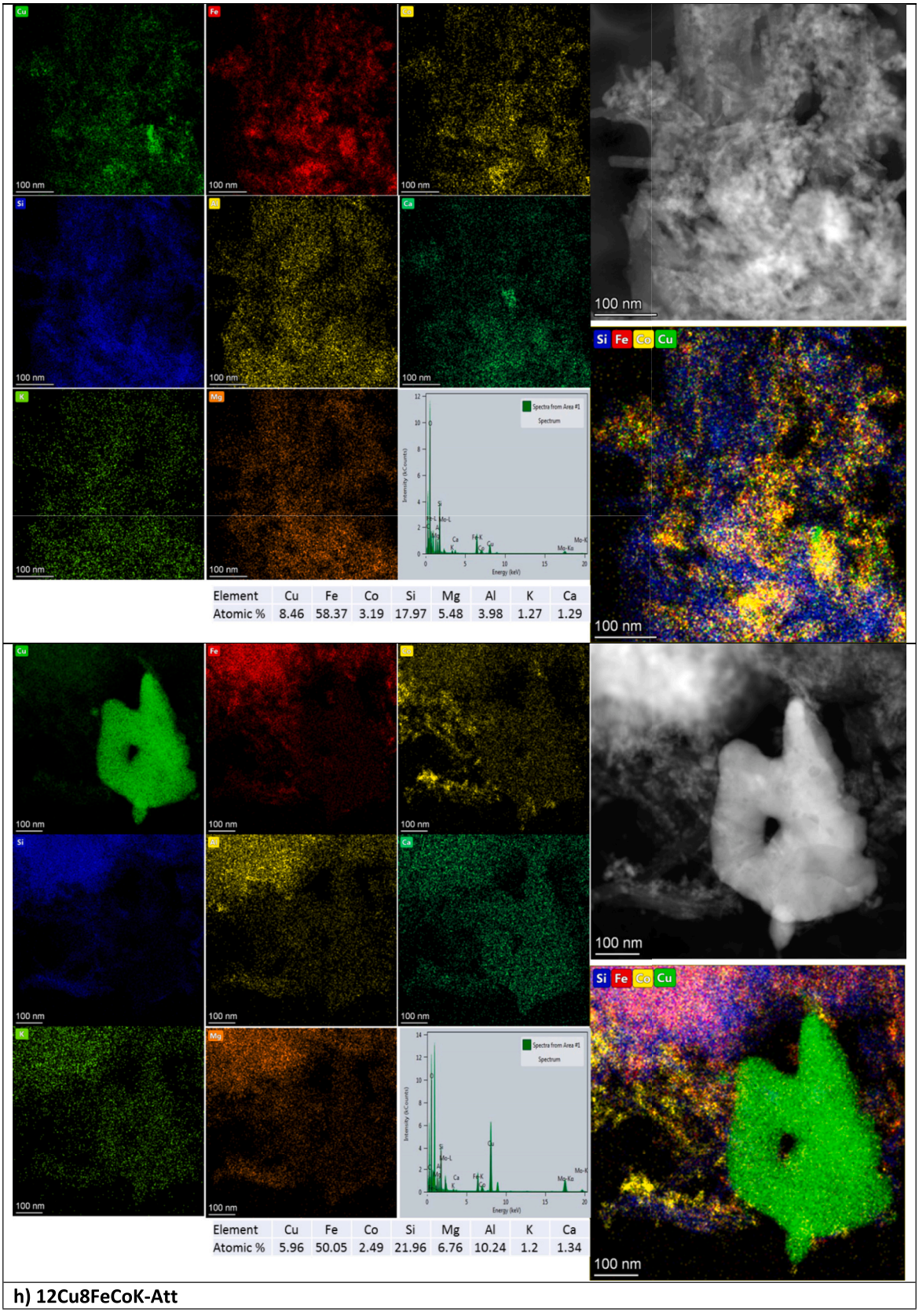

Fig. 19. (*continued*).

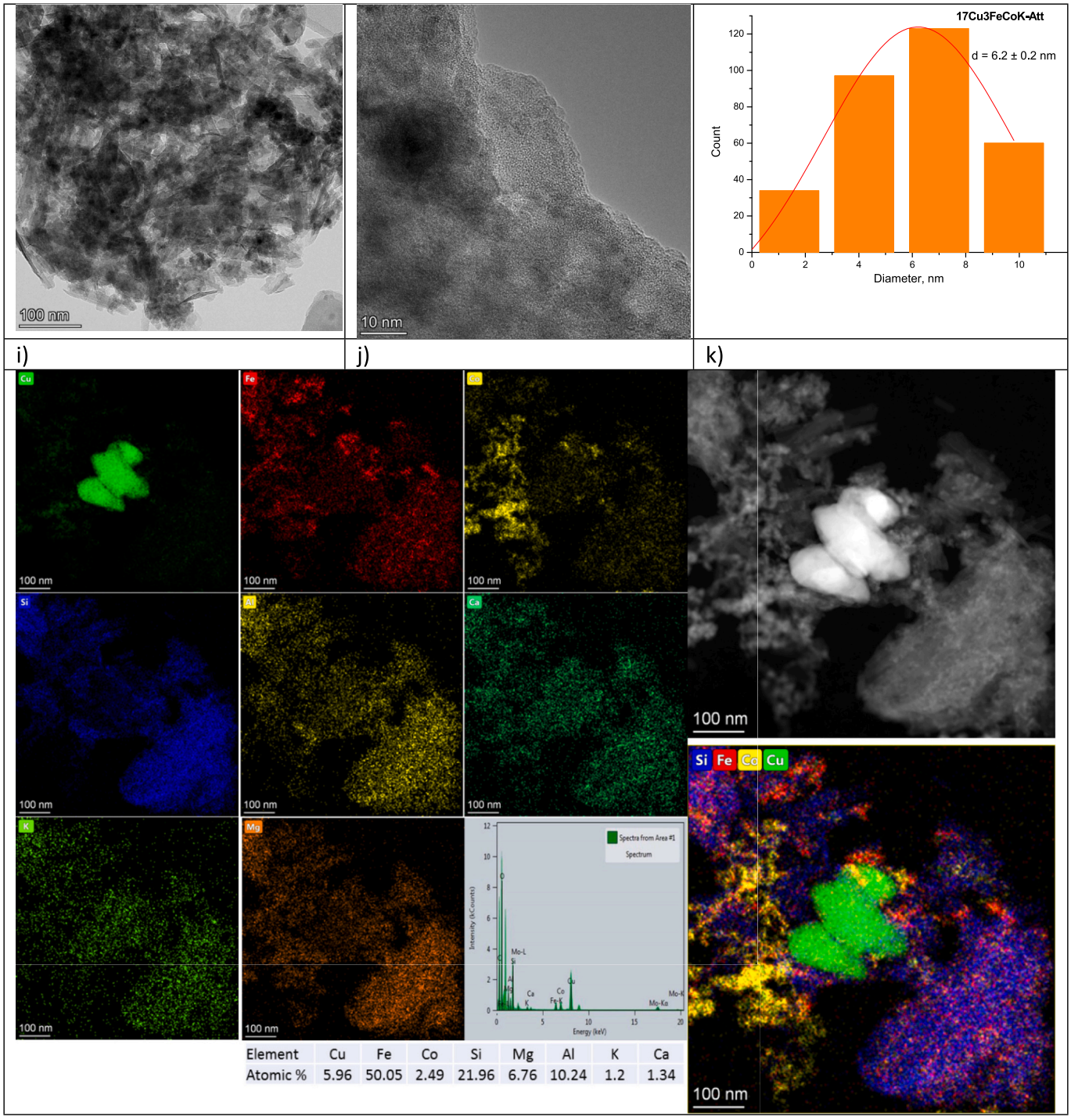

Fig. 19. (*continued*).

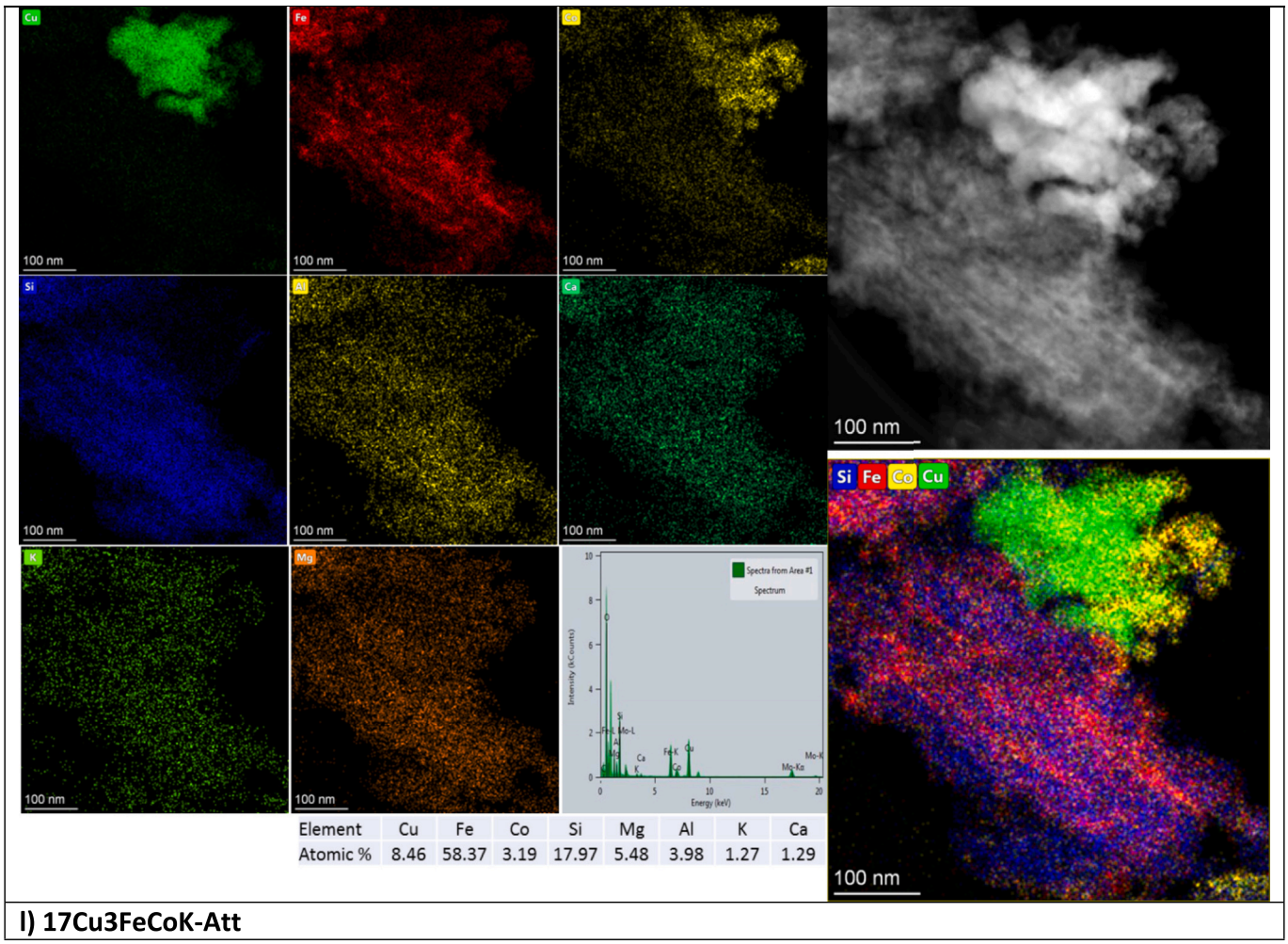

Fig. 19. (*continued*).

Cu_2O (PDF# 00-05-0661) with the average $D_{Cu2O} \sim 3$–4 nm. In addition to copper 12Cu8FeCoK exhibited reflexes at $2\Theta = 20.1^{o}$ attributed to Fe^0 (PDF N⁰ 00–006-0696, a = b = c = 2.866 Å) with the determined value of the lattice parameter a = 2.869(2) Å and the average CSD size D_{Fe} = 7.5 nm while the reflex from metallic iron Fe^o was not detected in 17Cu3FeCoK probably due to a low Fe loading in this catalyst. A more prominent reflex at 2Θ of 20.1° from Fe^0 (PDF N⁰ 00–006-0696, a = b = c = 2.866 Å) was obtained for the reduced iron-enriched 3Cu17FeCoK catalyst compared with 12Cu8FeCoK sample exhibiting the value of the lattice parameter a = 2.870(2) Å and the average D_{Fe} = 10.5 nm. There are also intense reflexes at 2Θ of 13.7°, 16.1°, 25.3°, 27.6° in 3Cu17FeCoK which can be attributed to two isostructural phases - a spinel-type structure magnetite Fe_3O_4 or $CuFe_2O_4$. The determined lattice parameter value *a* is equal to 8.386(3) Å. Note that it is not possible to distinguish Fe_3O_4 and $CuFe_2O_4$ phases directly from XRD pattern, however, comparison of XRD patterns of 3Cu17FeCoK and 12Cu8FeCoK samples presented in Fig. 18 allows to assume that the Fe_3O_4 phase is more likely to be formed based on a higher relative intensity of this peak at a lower copper content. The average CSD size of D_{Fe3O4} is 8 nm. Interestingly that similar crystal phases and trends were observed for the spent CuFeCo-based catalysts with different Cu/Fe ratio by Guo et al. [19]. The authors found that a decrease of the Cu/Fe ratio in the catalysts resulted in a significant decrease of Cu^0 and Cu_2O peaks intensities in XRD patterns, while on the contrary intensity of FeC_x and Fe_3O_4 (JCPDS, No. 84–0307) diffraction peaks gradually increased. It is worth noting, that the Fe^0 diffraction peak was not detected in the XRD patterns of spent CuFeCo-based catalysts attributed to the low reduction degree of iron oxides during the reaction [19]. Comparison of 2Θ values of XRD patterns in the current work and literature data, e.g. [19], should be carried out taking into account a difference in the wavelength values of X-ray diffraction sources of utilized diffractometers. It is also important to note that the attapulgite structure was not changed during catalyst preparation and activation under hydrogen (Fig. 18).

3.2.5. *TEM results*

TEM results along with HAADF-STEM images and EDX elemental mapping of reduced fresh catalysts are presented in Fig. 19. The average size of metal clusters was around 4–6 nm much lower than the size of average coherently scattering domains in XRD which could be anticipated. Uneven distribution of the elements on the surface of the support is also quite natural when active phases are deposited by impregnation due to intrinsic nonuniformity of the support surfaces.

Obviously because of different metal loading the extent of interaction between copper and iron is different in different catalysts as can be seen from the elemental mapping. Isolated copper domains are present in 17Cu3FeCoK-Att, while 12Cu8FeCoK-Att with the lowest average cluster size apparently has a higher degree of intimate contacts between copper and iron.

4. Conclusions

Synthesis of higher alcohols from syngas was performed in a fixed bed catalytic reactor at various temperatures (225–300 °C) and two different H_2:CO ratios, 2 and 1, over 3 different 22%-CuFeCoK/

attapulgite catalyst having different Cu:Fe ratios. It was found that the copper rich 17Cu3FeCoK/attapulgite catalyst generated more methanol than the other two catalysts, namely the 12Cu8FeCoK and 3Cu17FeCoK/attapulgite, which were instead more selective for production of higher alcohols with carbon numbers higher than 2.

Transformation rates for CO and hydrogen were found to increase with temperature and a higher H_2:CO ratio. The catalyst composition affected the rates in a way that the higher iron content and lower amounts of copper led to faster rates.

According to X-ray diffraction data 17Cu3FeCoK and 12Cu8FeCoK catalysts contain metallic copper and a highly dispersed crystal phase of Cu_2O. In 12Cu8FeCoK Fe^0 was present while such metallic iron Fe^0 was not detected in the catalyst with 17% Cu probably due to much lower Fe loading in this catalyst. The reduced iron-enriched 3Cu17FeCoK catalyst besides Fe^0 exhibited intense reflexes which can be attributed either to a more possible spinel-type structure magnetite Fe_3O_4 or $CuFe_2O_4$.

Selectivity to methane is influenced by the catalyst composition, namely a higher copper content can generate more methane at similar CO conversion. A hydrogen rich feed gas can even further increase selectivity of the undesired methane.

CRediT authorship contribution statement

Atte Aho: Writing – original draft, Investigation. **Noora Lind:** Investigation. **Pasi Virtanen:** Investigation. **Päivi Mäki-Arvela:** Writing – review & editing, Supervision, Methodology. **Kari Eränen:** Validation, Project administration, Methodology. **Sari Granroth:** Methodology, Investigation. **Ville Korpelin:** Investigation. **Karoliina Honkala:** Investigation. **Vincenzo Russo:** Formal analysis. **Irina Simakova:** Writing – review & editing, Investigation. **Dmitry Yu. Murzin:** Writing – review & editing, Project administration, Methodology, Conceptualization.

Declaration of competing interest

The authors declare that they have no known competing financial interests or personal relationships that could have appeared to influence the work reported in this paper.

Data availability

Data will be made available on request.

Acknowledgments

This work is part of the activities of the Johan Gadolin Process Chemistry Centre at Åbo Akademi University. Funding from Business Finland through the SynJet project is greatly acknowledged. Materials research infrastructure/Department of Physics and Astronomy, University of Turku is gratefully acknowledged for a possibility to use their XPS.

References

[1] Z. Li, Z. Zeng, D. Yao, S. Fan, S. Guo, J. Lv, S. Huang, Y. Wang, X. Ma, ACS Sust. Chem. Eng. 8 (2020) 200–209.
[2] G. Liu, G. Yang, X. Peng, J. Wu, N. Tsubaki, Chem. Soc. Rev. 51 (2022) 5606–5659.
[3] Z. Zeng, Z. Li, S. Guo, J. Lv, S. Huang, Y. Wang, X. Ma, ACS Sust. Chem. Eng. 9 (2021) 11258–11268.
[4] H.T. Luk, C. Mondelli, D.C. Ferré, J.A. Stewart, J. Pérez-Ramírez, Chem. Soc. Rev. 46 (2017) 1358–1426.
[5] M. Gupta, M.L. Smith, J.J. Spivey, ACS Catal. 1 (2011) 641–656.
[6] M. Suvarna, P. Preikschas, J. Pérez-Ramírez, ACS Catal. 12 (2022) 15373–15385.
[7] P. Preikschas, J. Bauer, K. Knemeyer, R.N. d'Alnoncourt, R. Kraehnert, F. Rosowski, Catal. Sci. Techn. 11 (2021) 5802–5815.
[8] W. Mao, J. Su, Z. Zhang, X.-C. Xu, W. Dai, D. Fu, J. Xu, X. Zhou, Y.-F. Han, Chem. Eng. Sci. 135 (2015) 312–322.
[9] J. Yu, D. Mao, L. Han, Q. Guo, G. Lu, Catal. Comm. 27 (2012) 1–4.
[10] Y. Liu, K. Murata, M. Inaba, I. Takahara, K. Okabe, Catal. Today 164 (2011) 308–314.
[11] I.C. ten Have, E. Valle, A. Gallo, J.L. Snider, M.S. Duyar, T.F. Jaramillo, Energy Tech. 7 (2019) 1801102.
[12] P.E. Boahene, V.R. Surisetty, R. Sammynaiken, A.K. Dalai, Top. Catal. 57 (2014) 538–549.
[13] E. Heracleous, E.T. Liakakou, A.A. Lappas, A.A. Lemonidou, Appl. Catal. Gen. 455 (2013) 145–154.
[14] Y. Wu, H. Xie, S. Tian, N. Tsubaki, Y. Han, Y. Tan, J. Molec. Catal. A: Chem. 396 (2015) 254–260.
[15] R. Xu, W. Wei, W. Li, T. Hu, Y. Sun, J. Molec. Catal. A: Chem. 234 (2005) 75–83.
[16] X. Han, K. Fang, Y. Sun, RSC Adv. 5 (2015) 51868–51874.
[17] B. Liu, Y. Li, Y. Duan, T. Ding, Y. Tang, C. Zheng, React. Kinet. Mech. Cat. 128 (2019) 695–706.
[18] Y. Lu, F. Yu, J. Hu, J. Liu, Appl. Catal. Gen. 429–430 (2012) 48–58.
[19] H. Guo, H. Zhang, F. Peng, H. Yang, L. Xiong, C. Wang, C. Huang, X. Chen, L. Ma, Appl. Catal. A: Gen.l 503 (2015) 51–61.
[20] J.-L. Cao, G.-S. Shao, Y. Wang, Y. Liu, Z.-Y. Yuan, Catal. Comm. 9 (2008) 2555–2559.
[21] H. Chen, A. Wang, J. Coll. Interf. Sci. 307 (2007) 309–316.
[22] J.M. Huggett, in: R.C. Selley, L.R.M. Cocks, I.R. Plimer (Eds.), Encyclopedia of Geology, Elsevier, Oxford, 2005, pp. 358–365.
[23] M. Luo, H. Hamdeh, B.H. Davis, Catal. Today 140 (2009) 127–134.
[24] N. Gong, Y. Wu, Q. Ma, Y. Tan, Catalysts 13 (2023) 237.
[25] C. Huang, C. Zhu, M. Zhang, J. Chen, K. Fang, Appl. Catal. Environ. 300 (2022) 120739.
[26] Y. Ge, T. Zou, A.J. Martín, T. Block, R. Pöttgen, J. Pérez-Ramírez, Chem Catalysis. (2024), https://doi.org/10.1016/j.checat.2024.101010.
[27] Y. Ge, T. Zou, A.J. Martín, J. Pérez-Ramírez, ACS Catal. 13 (15) (2023) 9946–9959.
[28] J. Xu, J. Wei, J. Zhang, N. Liu, Q. Ge, J. Sun, Chem Catalysis 3 (4) (2023).
[29] T. Qin, T. Lin, X. Qi, C. Wang, L. Li, Z.L. Tang, L. Zhong, Y. Sun, Appl. Catal. Environ. 285 (2021) 119840.
[30] M. Ding, L. Ma, Q. Zhang, C. Wang, W. Zhang, T. Wang, Fuel Process. Techn. 159 (2017) 436–441.
[31] chemstations.com, (2024).
[32] D. Förtsch, K. Pabst, E. Groß-Hardt, Chem. Eng. Sci. 138 (2015) 333–346.
[33] M.C. Biesinger, B.P. Payne, A.P. Grosvenor, L.W.M. Lau, A.R. Gerson, Smart Appl. Surf. Sci. 257 (2011) 2717–2730.
[34] T. Grzybek, H. Papp, N. Baerns, Appl. Catal. 29 (1987) 335–350.
[35] M.C. Biesinger, L.W.M. Lau, A.R. Gerson, R.St.C. Smart, App. Surf. Sci. 257 (2010) 887–898.
[36] E. Paparazzo, J. Electron Spectr. Related Phenom. 43 (1987) 97–112.
[37] R. Zhu, K. Wang, Y. Xing, C. Li, X. Gao, Q. Ma, T.-S. Zhao, J. Zhang, New J. Chem. 48 (22) (2024) 9920–9930.
[38] V.L. Kuznetsov, D.V. Krasnikov, A.N. Schmakov, K.V. Elumeeva, Phys. Status Solidi B 249 (12) (2012) 2390–2394.
[39] M. He, M. Luo, P. Fang, J. Rare Earths 24 (2006) 188–192.
[40] R. Khunphonoi, P. Khemthong, C. Luadthong, S. Kuboon, C. Kongmark, N. Viriya-empikul, P. Kidkhunthod, S. Pinitsoontorn, K. Faungnawakij, RSC Adv. 12 (2022) 15526–15533.
[41] J. Zhu, J. Yu, L. Zhu, X. Yu, J. Liu, Y. Chao, J. Yin, P. Wu, J. Liu, W. Zhu, New J. Chem. 48 (2) (2024) 898–909.